

Magnetic resonance imaging for detection and analysis of mouse phenotypes

Brian J. Nieman,^{1,2*} Nicholas A. Bock,^{1,2} Jonathon Bishop,¹ X. Josette Chen,^{1,2} John G. Sled,^{1,2} Janet Rossant^{3,4} and R. Mark Henkelman^{1,2}

¹Mouse Imaging Centre, Hospital for Sick Children, Toronto, Canada

²Department of Medical Biophysics, University of Toronto, Toronto, Canada

³Samuel Lunenfeld Research Institute, Mount Sinai Hospital, Toronto, Canada

⁴Department of Molecular and Medical Genetics, University of Toronto, Toronto, Canada

Received 5 April 2005; Revised 30 June 2005; Accepted 7 July 2005

ABSTRACT: With the enormous and growing number of experimental and genetic mouse models of human disease, there is a need for efficient means of characterizing abnormalities in mouse anatomy and physiology. Adaptation of magnetic resonance imaging (MRI) to the scale of the mouse promises to address this challenge and make major contributions to biomedical research by non-invasive assessment in the mouse. MRI is already emerging as an enabling technology providing informative and meaningful measures in a range of mouse models. In this review, recent progress in both *in vivo* and *post mortem* imaging is reported. Challenges unique to mouse MRI are also identified. In particular, the needs for high-throughput imaging and comparative anatomical analyses in large biological studies are described and current efforts at handling these issues are presented. Copyright © 2005 John Wiley & Sons, Ltd.

KEYWORDS: MRI; mouse imaging; phenotype; multiple mouse MRI

INTRODUCTION

The mouse has become the most popular mammal for biomedical research. This is not only a result of its small size and rapid life cycle – which make the mouse more economical and convenient than larger animals – but also because of the development of genetic information and manipulation technology for the mouse. With data in hand from the human¹ and mouse² genome projects, a wealth of information is available about the genes that define them. The extensive genetic similarities² between the mouse and the human make the mouse an excellent model for understanding common developmental processes and pathologies in the human. Individual genes from the mouse can be altered, deleted or replaced through targeted genetic manipulations.³ Additional genes can be added through the expression of transgenes. Combining these genetic tools with the array of manipulable environmental factors allows tremendous flexibility in experiment design. This provides an unprecedented level of experimental control for interrogating the complex relationships between genes, environment, organism development and mechanisms of disease.

Ultimately, for insight gained from the laboratory mouse to improve our understanding of the human and positively influence the course of human diseases, accurate models of these conditions in the mouse must be developed. For this reason, large-scale efforts are under way to identify and study models of human diseases in the mouse. Several strategies have been implemented for the production of mutant mice. In cases where particular genes are already implicated, targeted genetic alterations may produce realistic models of the human condition. Alternatively, efficient and less labor intensive means exist to mutate the mouse genome and subsequently screen for phenotypes directly related to the human disease of interest. Chemical mutagenesis by agents such as *N*-ethyl-*N*-nitrosourea (ENU), for instance, can produce large numbers of random point mutations.^{4–6} Such random mutagenesis techniques offer full genome coverage and rapid means of unbiased genetic screening. Intermediates between random and targeted techniques, most notably gene-trap insertional mutagenesis, have also been implemented.^{7,8} The importance of mouse models generated by each of these methods cannot be overestimated. Even in cases where a disease model can be induced by experimental procedures, such as xenograft models of cancer or surgically induced infarctions, the sensitization or protective effect of a genetically modified background provides valuable insight into the mechanisms of disease or potential therapies. Independent of the particular disease or experimental model,

*Correspondence to: Brian J. Nieman, Mouse Imaging Centre, Hospital for Sick Children, 555 University Avenue, Toronto, Ontario, Canada M5G 1 × 8. E-mail: brian.nieman@sw.ca

Contract/grant sponsors: Canada Foundation for Innovation/Ontario Innovation Trust; Ontario Research and Development Challenge Fund; National Institutes of Health; Canadian Institutes of Health Research; Genome Canada; Burroughs Wellcome Fund.

it is paramount that investigations include systematic observation and characterization of mouse phenotype for meaningful comparisons between experimental groups.

We define here a phenotype as an observable anatomical, biochemical or functional state of an individual. The goal of mouse phenotyping is therefore to answer the question, 'what is different about this mouse compared with some standard mouse?' This difference is the result of the ensemble of genetic and environmental conditions that influence each mouse's development. A thorough understanding of a mouse phenotype and its correlation to similar human conditions is the research question of primary interest in the search for experimental models of human disease. The observation of identified phenotypes under controlled experimental conditions may provide fundamental insight into the mechanisms of disease processes or appropriate treatments. Phenotypic information regarding anatomical structure or function may need to be compared or tracked over time, perhaps in both the presence and absence of different pharmacological agents or treatment regimens. Description and quantification of mouse phenotype are critical to these experimental designs.

With this definition of a mouse phenotype, many of the diagnostic techniques from clinical medicine can also be applied in the mouse. These include the imaging tools that have become critical in the diagnosis of human conditions. Magnetic resonance imaging (MRI) in particular permits the assessment of disease state throughout the body, guiding therapeutic decisions and evaluating responses over time. Existing imaging protocols allow a range of both structural and functional information to be drawn from imaging data sets. Similar information is required in characterizing and identifying abnormal mouse phenotypes. Consequently, biomedical research centers throughout the world are adapting human MRI techniques down to the scale of the mouse.

In spite of some challenges, MRI is well suited to scale in size from human to mouse imaging. The major challenge is obtaining images with comparable signal-to-noise ratio (SNR) and resolution as human clinical scans but at the mouse scale, where voxel dimensions must be decreased by a factor of 10–15-fold in each dimension. Several modifications to scanner hardware and imaging protocols are commonly implemented to offset the loss in SNR accompanying this decrease in scale. The design and construction of specialized mouse radiofrequency coils greatly increase the sensitivity to the MR signal and represent the single largest recovery in SNR. Additional gains – at least linear with resonance frequency – are seen in moving to higher field strengths (up to as high as 17.6 T⁹). Any remaining SNR deficit can generally be recovered by increasing the scan duration, which is well tolerated in anesthetized mice up to a maximum of ~3 h. With these modifications, high-quality mouse MR images can be obtained very reliably.

This review is intended to give the reader a current perspective on the adaptation of clinical MRI to biomedical research in the mouse. Emphasis is placed on the variety and types of phenotyping that can be achieved by MR methods. The paper is organized into several parts. The first section is dedicated to recent experimental progress and developments in mouse MRI with regard to phenotyping techniques. This section largely highlights the successes in adapting human MRI protocols – clinical and research – to the mouse scale. It is subdivided into several smaller sections: anatomical imaging; functional imaging; high-resolution fixed mouse imaging; cancer studies; and MR spectroscopy. Some of the MR challenges unique to mouse imaging in biomedical research are also considered. These areas include increasing image throughput and analyzing anatomical images from multiple-mouse data sets. Throughout, the review has been restricted primarily to mouse imaging, focusing on studies of development and disease in genetically modified mice and the technical achievements aimed at enabling such studies.

RECENT PROGRESS

Anatomical imaging

The anatomical visualization of soft tissue has long been a great strength of MRI. This continues to be its most valuable clinical role. The ability to 'see' the state of tissue or to assess the extent of disease is of critical importance. This is also true in mouse MRI, where the *in vivo* visualization of tissue allows for quantitative comparison between control and experimental groups and also for monitoring over the course of longitudinal studies. The flexibility of MRI in generating differential contrast – both endogenous and contrast agent induced – can be used to great advantage for the emphasis of various anatomical features or pathologies of interest.

One of the most popular murine organs to be studied anatomically is the brain. This follows the initial focus of clinical MRI on the human brain and reflects the importance and difficulty of assessing brain diseases in the human population. Fortunately, the brain is one of the easier parts of the mouse to image as motion artifacts can be largely eliminated by the use of head restraints.^{10–12} This allows very high-resolution imaging through efficient use of extended scan durations. High-resolution scans, preferably three-dimensional and isotropic, are critical if delineation of small structures is required.¹³ Figure 1, for example, demonstrates improvements in visualization of brain structure with increasingly isotropic three-dimensional voxels.

Anomalous shape, appearance or volume of brain structures is commonly indicative of abnormal development or disease state. Comparison of mutant and control mouse anatomy reveals the effect of altered genetics and

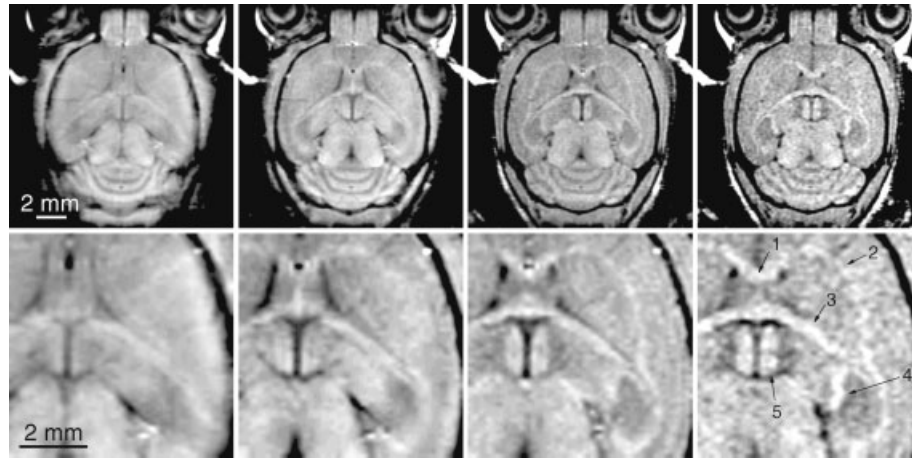


Figure 1. Improved visualization of brain structures with reduction of through plane partial volume effects as demonstrated by Natt *et al.*¹³ Top: T_1 -weighted 3D MRI images of the mouse brain *in vivo* with decreasing voxel size from left to right. The voxel size decreases from $117 \times 117 \times 938 \mu\text{m}$ to $117 \times 117 \times 469 \mu\text{m}$, $117 \times 117 \times 234 \mu\text{m}$ and $117 \times 117 \times 156 \mu\text{m}$. Bottom: magnified views showing the (1) corpus callosum, (2) external capsule, (3) fimbria hippocampi, (4) hippocampal formation and (5) medial habenular nucleus. Reprinted from Reference 13 with permission from Elsevier

hence can be used to assess mouse phenotype. Imaging studies can be supplemented and coordinated with related functional or behavioral studies. For example, a decreased hippocampal volume and associated cognitive impairments (as measured by an eye blink conditioning experiment) have been demonstrated¹⁴ in mice overexpressing amyloid precursor protein (APP), a model of Alzheimer disease. These measures accurately reflect the human condition both anatomically and behaviorally, suggesting this is a good model for studying disease development and possible therapies. In fact, transgenic mouse models continue to be critical to our developing understanding of Alzheimer disease and MRI can play an important role through non-invasive assessment. However, in other cases, MR images of mutant mice may uncover phenotypes that appear inconsistent with the human disease or show unexpected abnormalities. This has been the result with the fragile X knockout mouse¹⁵ (modeling fragile X syndrome) and the *dy/dy* mouse¹⁶ (modeling merosin-deficient muscular dystrophy) as examples, which fail to show the expected hypoplasia in the cerebellar vermis and MR changes in periventricular white matter, respectively. These anatomical differences are important in understanding the pathogenesis of both human and mouse disease. In addition to comparing between groups of mice, tracking changes longitudinally enables an assessment of disease evolution. For instance, the volumes of several brain structures have been monitored over time in a mouse model of megencephaly,¹⁷ revealing that increased growth in this model is largely restricted to particular brain structures and becomes evident in early disease stages at 8 weeks and onwards. Temporal evaluation of the mouse phenotype by MRI thus allows the investigation of events throughout progression of disease.

In addition to genetic mouse models, experimentally induced models of human diseases have been established in the brain and elsewhere. We note that while some of these models – particularly surgically induced models – are more easily performed in larger animals such as the rat, the genetic manipulation tools available in the mouse make it an attractive system. For example, certain genetically modified animals, such as the apolipoprotein E knockout (ApoE^{-/-}) mouse, are more sensitive to surgically induced cerebral ischemia.¹⁸ A preliminary study¹⁹ has temporally monitored neurodegeneration in this model by measuring atrophy on MR images and comparing with control mice. Such studies will allow an improved understanding of the role of genetic interactions in non-heritable diseases and similar experimental models. Likewise, investigations of viral infection in the mouse are also of great interest^{20–25} as lesions can be observed longitudinally using MRI.²³ This approach has been used in the study of herpes simplex virus.^{20–22,25} Interestingly, in this model, *in vivo* MRI shows progression of MR signal abnormalities despite improvement of clinical symptoms and low viral load,²¹ indicative of secondary mechanisms of tissue damage. Future studies including the use of genetically modified mice may shed light on these secondary effects and improve recognition and treatment of equivalent human conditions.

In all of these studies, different MR contrast may be used to highlight the anatomy or pathology of interest. While T_1 - or T_2 -weighted images are most common, alternative sequences allowing more detailed quantitation or alternative endogenous contrasts such as magnetization transfer,²⁶ $T_{1\rho}$ ^{27,28} or others²⁹ have also been successfully applied to the mouse brain. Mouse models prove valuable in assessing the diagnostic utility of such techniques. As an example, quantitative mapping of parameters such as

T_1 or T_2 may be more sensitive to subtle differences than imaging alone. Subtle changes in T_2 distinguish transgenic models of Alzheimer disease.^{30,31} These measures may become more commonplace in mouse phenotyping than in human diagnostics since mouse populations are genetically homogeneous and exhibit a smaller population variance. Other techniques finding particular utility include diffusion-weighted imaging. Diffusion tensor imaging (DTI) in particular provides important insight into the local tissue state. *Shiverer* mice, for instance, which lack myelin basic protein, have an increased water diffusion perpendicular to the direction of fiber tracks in the brain³² consistent with the expected absence of myelin. Studies of altered diffusion in models of cerebral ischemia^{33,34} and Alzheimer disease^{35,36} have also been used in tracking regions of brain damage and assessing the extent of brain disease.

Exogenous contrast agents may likewise be used to advantage in the study of the anatomy of the brain. Notably, manganese (typically in the form of $MnCl_2$), a T_1 -shortening contrast agent generally unusable in human studies owing to toxicity, has become important in mouse imaging. Manganese is a calcium analog and is taken up through the same channels. It is tolerated in low doses³⁷ and differentially stains specific cell layers and anatomical regions. In particular, regions of the cerebellum, hippocampus and olfactory bulbs and also the pituitary gland, pineal gland and choroid plexus enhance significantly.^{38–40} An example mouse brain image is provided in Fig. 2. Alternatively, small amounts of manganese can be injected at a site of interest and allowed to transport along axonal tracks. Imaging then highlights the connectivity within the brain.^{13,41,42} Other contrast agents are designed with specific targets. Development of contrast agents to detect amyloid plaque burden^{43,44} – difficult to achieve with endogenous contrast^{45–47} – is one example shown in Fig. 3. Preliminary work in this area has focused on studies in transgenic APP mice and has obvious research and clinical applications. Mouse models provide a means for preclinical trials of such agents and

are especially suited to test targeted, disease-specific contrast agents which may subsequently be used to assess human treatment or progression studies.

One particularly active area of contrast agent development at this time is aimed at the magnetic labeling and tracking of cells. This technology will have important implications for monitoring cell therapy or investigating the role of migrating cell populations in disease development. Several experiments in the mouse have reported observation of labeled cells for studies in the brain,^{48,49} spine,⁵⁰ pancreas,⁵¹ spleen⁵² and heart.⁵³ Research aimed at the development of these contrast agents as well as cell-labeling strategies continues.^{54–58} Additional flexibility is available to research applications by use of genetically modified cells and animals. For instance, iron-regulating genes can be modified to promote selective accumulation of endogenous iron⁵⁹ or specific receptors can be expressed and used in combination with antibodies conjugated to MR contrast agents.^{60–63} It is possible that such genetic manipulation will permit not only cell tracking but also MR visualization of gene expression. These significant developments will broaden the role for MRI in biomedical research, but are not considered in further detail here.

Other parts of the body or indeed the whole mouse can also be studied by MRI. Whole-body studies to date include quantification of fat distribution⁶⁴ with the aim of elucidating genetic origins and improving treatments of obesity. Smaller scale imaging of the kidneys,^{65–67} the spinal cord,⁶⁸ the knee joints^{69,70} and even the mouse adrenals⁷¹ has been performed. A good example of one of the more challenging pathologies to assess in the mouse is atherosclerosis. The small size of mouse blood vessels and the rapid heart rate generally necessitate both high-resolution imaging and motion compensation techniques such as prospective gating. The prevalence of human vascular disease, however, motivates a large effort in developing effective means of assessing and understanding related mouse models.⁷² An important model in these studies is the $ApoE^{-/-}$

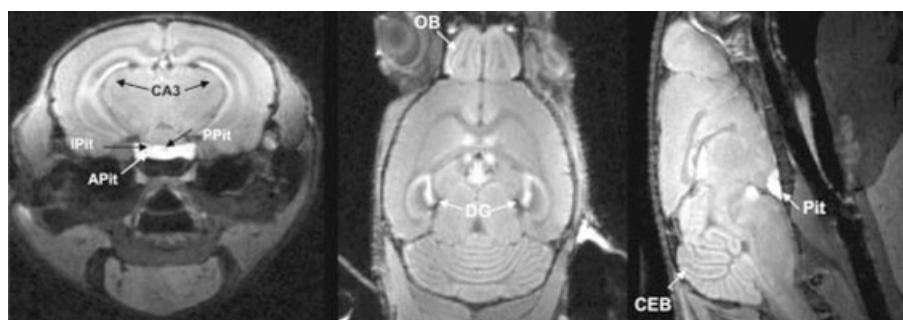


Figure 2. High-resolution ($100 \times 100 \times 100 \mu m$), T_1 -weighted three-dimensional manganese-enhanced MRI of the mouse brain as demonstrated by Silva *et al.*³⁷ Transverse (left), coronal (middle) and sagittal (right) views, showing contrast due to the presence of Mn^{2+} in regions such as the hippocampus (CA3 and DG), pituitary gland (Pit) and its major lobes (APit, IPit, PPit), cerebellum (CEB) and olfactory bulb (OB). Reprinted from Reference 37 with permission from John Wiley & Sons, Inc.

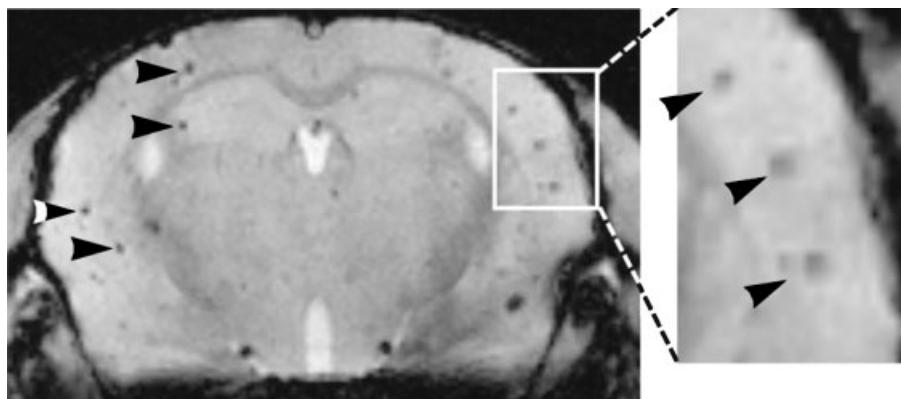


Figure 3. Detection of $A\beta$ plaques with *in vivo* MRI and targeted contrast agents. Following injection of Gd-DTPA- $A\beta$ 1–40 with mannitol, *in vivo* T_2^* -weighted MR images ($TE = 15$ ms, $TR = 1.5$ s, $78 \times 78 \times 250 \mu\text{m}$, 59 min imaging time) show $A\beta$ plaques in a 6-month-old APP/PS1-transgenic mouse brain. Arrowheads indicate $A\beta$ plaques that corresponded to stained plaques in histology sections. Image courtesy of Wadghiri *et al.*⁴⁴ Reprinted from Reference 44 with permission from John Wiley & Sons, Inc.

mouse. Using this model, several studies have established the potential of MRI to detect atherosclerotic lesions.^{73–76} The development of atherosclerosis has been monitored longitudinally in the mouse aorta;^{77,78} atherosclerosis can be observed beginning at about 20 weeks in these mice and progression can be observed through arterial wall remodeling.⁷⁷ Successful detection of atherosclerosis has also been demonstrated in other relevant mouse models⁷⁹ and in a variety of blood vessels^{79,80} (see Fig. 4). Good correlations with more traditional histology methods have been observed,^{73,74,81} thus supporting the utility of MRI in future longitudinal genetic and treatment studies.

Detailed volume measurements or observations of morphology from anatomical mouse MRI are powerful

in vivo assessments of developmental abnormalities or the extent of disease. Straightforward quantification and comparison of multiple experiment groups in biomedical research studies can be accomplished in this manner. Imaging protocols can be kept simple and efficient. For this reason, mouse MRI will have a growing role as a tool for the visualization of anatomical structures and pathology in the characterization of individual mutants and in large-scale screening projects.

Functional MRI

MRI not only provides for anatomical visualization, but also allows a number of functional studies. The data

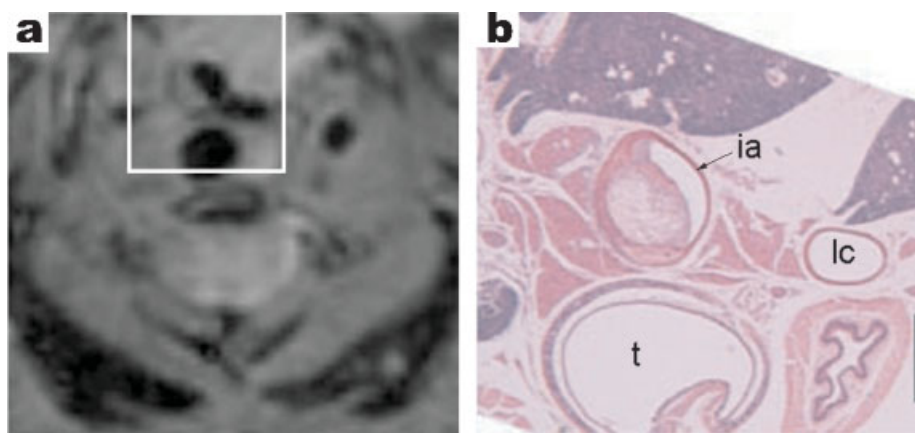


Figure 4. *In vivo* MR visualization of atherosclerosis in low-density lipoprotein-deficient ($LDLR^{-/-}$) mice as demonstrated by Hockings *et al.*⁷⁹ In (a), plaque deposition in the innominate artery is visible by MRI using an FSE sequence with fat suppression. The white box indicates the corresponding region in the histological section (b). The innominate artery (ia), trachea (t) and left carotid artery (lc) are labeled in (b). The scale bar indicates $500 \mu\text{m}$. Reprinted from Reference 79 with permission from Lippincott, Williams & Wilkins

collection and analyses are often more complicated in functional imaging experiments, particularly since anesthetic effects may be a confounding factor.⁸² However, the additional information allows the scientist to assess more thoroughly how genetic alterations or disease may affect the whole animal. Many functional assessments depend on hemodynamic responses, including measurements of perfusion, blood flow and blood oxygenation. Cardiac functional measurements take on a different form, with measurements of performance typically derived from the motion of the heart through a dynamic sequence of images covering the entire heart cycle.

Several functional imaging techniques are designed to monitor hemodynamic responses. These include studies of perfusion, cerebral blood volume (CBV) or flow (CBF) and blood oxygenation level-dependent (BOLD) effects. Diseases where blood supply or oxygenation levels are at risk are therefore of particular interest. Again, studies of brain diseases are the most frequent reports of these types in the literature. Surgically-induced cerebral ischemia can be monitored in this fashion and the dynamics of diffusion and/or perfusion tracked and compared amongst mice with the aim of improving therapeutic strategies.^{83–85} Altered perfusion has also been reported in heritable diseases, such as in the case of sickle cell disease where hypoxic regions at risk of vaso-occlusion may be identified.^{86,87} Mutant APP mice are again an interesting case. Cerebral blood volume reduction,⁸⁸ compromised hemodynamic response⁸⁹ and flow disturbances⁹⁰ have been monitored by MRI; compromised performance is observed in aged mice but not in young mice. Further study of the vasculature by MR angiography and corrosion casts reveal significant defects including vessel rearrangements and substitutions that begin at about 7 months of age.⁹⁰

Functional imaging of hemodynamic responses to neuronal activation in the murine brain is also possible, although the need to anesthetize mice during imaging limits the possible experiments in mice compared with humans. Nevertheless, studies have measured significant BOLD or CBV effects in traditional fMRI experiments using alternating blocks of sensory stimulation and rest periods during light anesthesia. For example, regions of activation in the somatosensory cortex have been examined by BOLD-fMRI with electrical somatosensory stimulation of the hindpaw,^{91,92} as demonstrated in Fig. 5. Such studies can be implemented in transgenic animals to study functional deficits. An age-dependent impairment of a somatosensory response in transgenic APP mice has been demonstrated⁹³ with CBV-fMRI. Other means of fMRI are also being evaluated, including studies with pharmacological stimulation.⁹⁴ One attractive alternative uses manganese to stain preferentially regions of increased neuronal activity during repeated performance of a task or exposure to a stimulus (with or without anesthesia). Active regions can subsequently be observed as enhancements on MR images where active calcium channels have taken up manganese. Experiments

in the olfactory bulbs of mice have been successful at delineating regions of the olfactory system sensitive to particular odors in this manner.⁹⁵ This presents a potentially simpler and equivalent technique to fMRI methods (which have also been tested in the olfactory system⁹⁶).

Functional measurements of the heart are challenging in the mouse. However, overcoming this challenge has permitted not only functional heart measurements but also imaging of atherosclerosis, coronary arteries⁹⁷ and other regions of anatomy prone to artifacts from cardiac and/or respiratory motion. As the mouse heart beats at a rate of around 500 bpm, fast gradient hardware and fast sequences are required to compensate for these motion effects. This can be accomplished with smaller, mouse-dedicated gradient coils. Monitoring and triggering can then proceed in a manner analogous to human cardiac imaging. This permits very high-resolution imaging in the mouse heart from which functional performance can be assessed. In this fashion, normal development of the heart can be monitored in mice from a very early age and quantified longitudinally,⁹⁸ as demonstrated in Fig. 6.

Likewise, the heart can be examined in various states of disease. Experimentally-induced myocardial infarctions are an example; detailed measurements of ventricular mass, ejection fraction and wall thinning assess the effect of the infarct and also subsequent ventricular remodeling.^{99–103} Such measurements ideally require high-quality three-dimensional representations of the beating heart,¹⁰⁴ data difficult to obtain by any methods other than MRI. Further assessment can be made by pharmacological stress testing of the heart with an agent such as dobutamine; the ability to increase cardiac output is lost in chronically infarcted myocardium.¹⁰⁵ Further studies of the effects of genetic alterations on heart performance can be accomplished by the same techniques. For example, cardiac deficiencies in ejection fraction and wall thickness have been quantified in mice with a ventricular specific knockout of vascular endothelial growth factor A.¹⁰⁴

Interestingly, cardiac functional studies of this kind may also benefit from manganese-enhanced imaging since manganese can be a marker of calcium flux in the heart. Changes in cardiac function by increased or decreased inotropy after administration of dobutamine or diltiazem, respectively, are accompanied by associated larger or smaller signal intensity increases in the presence of manganese.¹⁰⁶ Similarly, alterations in signal enhancements in the infarcted heart may reveal regions of viable and infarcted tissue.¹⁰⁷

Tagged cardiac imaging or other displacement encoding techniques can also be performed in the mouse to supplement standard cine imaging. In these studies, a periodic signal-intensity pattern such as a grid is generated over the heart, allowing visualization of wall deformation during myocardial contraction. Calculations from the resulting images map parameters such as stress and strain within the ventricular wall,^{108,109} parameters unavailable without myocardial tagging. Experiments have

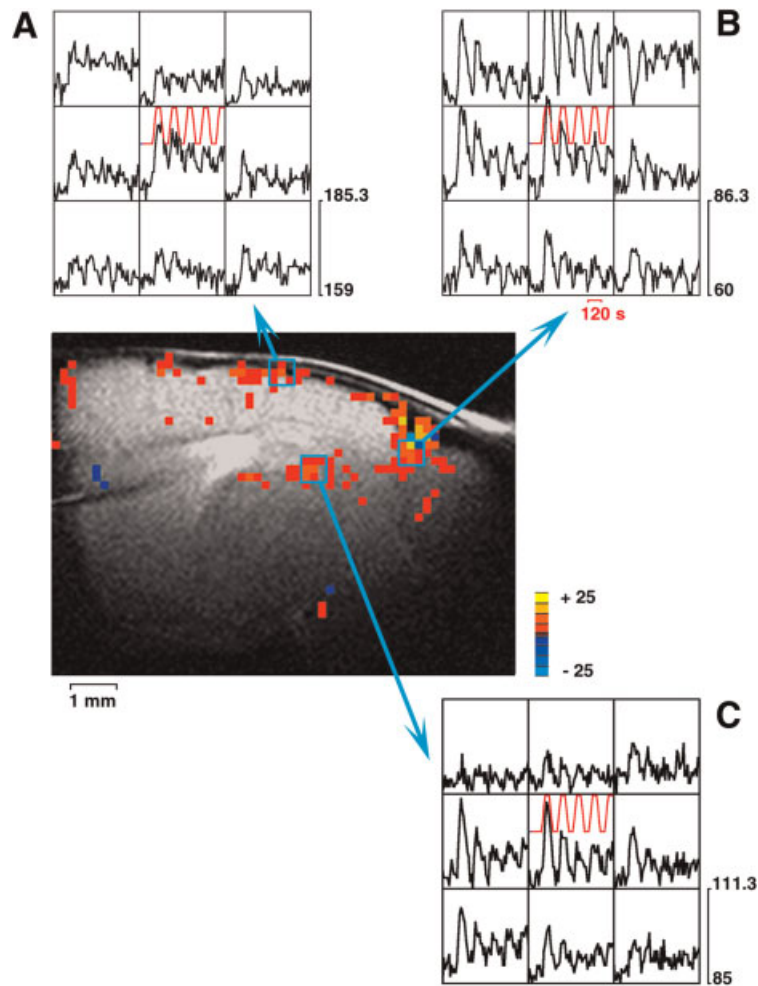


Figure 5. BOLD-fMRI in the mouse brain during electrical somatosensory of the hindlimb. The time course of voxel intensity is shown in the somatosensory regions (A) and in draining veins (B, C). Images are courtesy of Ahrens and Dubowitz.⁹¹ Reprinted from Reference 91 with permission from John Wiley & Sons, Inc.

successfully demonstrated dysfunction in the infarcted murine heart both at the site of infarct and in surrounding regions.¹¹⁰ The additional information from these techniques complements analysis of cine images.

Functional measurements in mouse models are powerful means of quantitatively assessing the state of tissue in mouse models of human disease. Although functional imaging protocols are usually more complicated, the measurements they provide non-invasively are often not otherwise accessible. Functional imaging is therefore likely to continue to have an important role in the characterization of particular disease models and monitoring of changes produced by therapeutic interventions.

High-resolution fixed mouse imaging

The resolution of *in vivo* imaging is limited by the length of time that mice can be kept safely anesthetized and by physiological motion during the imaging session.

Although hardware and pulse sequence developments continue to improve image quality, three-dimensional visualization is sometimes desired at higher resolutions than can be achieved *in vivo* or over extended parts of the mouse normally compromised by motion artifact. In biomedical research, such images can still be achieved by imaging mice *post mortem* following fixation. This is particularly advantageous for imaging individual organs *ex vivo*, but in fact the entire mouse can be well imaged by this method. Such an imaging session can be added at the conclusion of existing *in vivo* studies and offers superior anatomical and morphological MR visualizations prior to or for the guidance of conventional histological analyses.

Embryonic imaging is a good example of the advantages of MRI of specimens following fixation. Owing to the small size and frequent motion of the embryo, it is very difficult to image *in utero* by MRI methods.^{111,112} Imaging fixed embryo specimens can in contrast achieve very high resolution.^{113,114} Dhenain *et al.*¹¹³ were thus

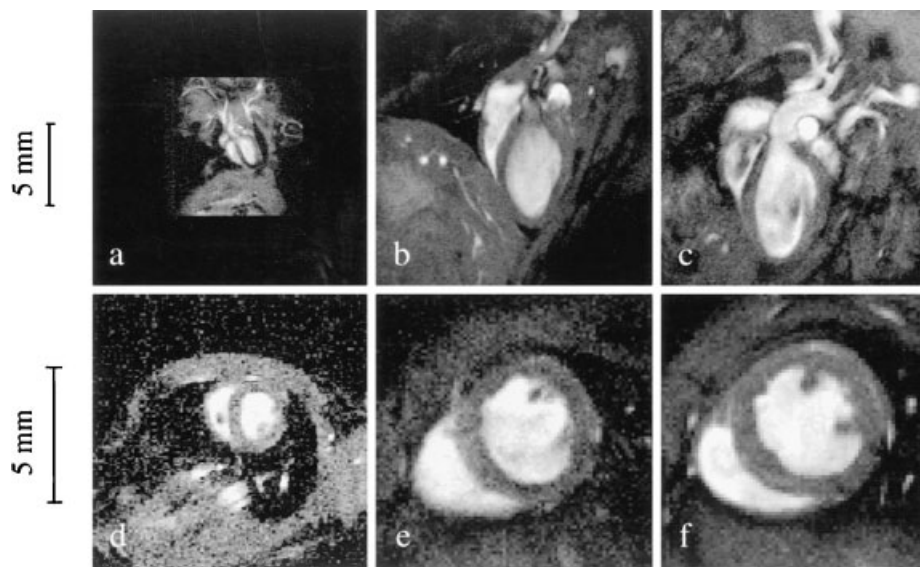


Figure 6. Cine MR images at end diastole in 3-day (a), 3-week (b) and 5-week (c) old mice. Short-axis images at a midventricular level are shown in (d)–(f). Images courtesy of Wiesmann *et al.*⁹⁸ Reprinted from Reference 98 with permission from The American Physiological Society

able to create a digital atlas of the embryo with images from 6 to 15.5 days post-conception. Resolution in these images was as high as 20 μm in the smallest embryos and displays detail that cannot be obtained *in vivo*. In order to achieve this resolution, scan times were as long as 37 h at 11.7 T. Example embryo images are provided in Fig. 7.

Similar motion challenges exist for *in vivo* DTI, owing to the need to acquire diffusion-weighted three-dimensional images in multiple directions and the inherent aberrations due to organ motion. Initial DTI studies of *in vivo* and fixed mouse brains indicate that, even though absolute diffusion is substantially reduced by the fixation process, relative indices such as the fractional anisotropy and the radial and axial trace-normalized diffusivities are conserved.^{115,116} Lengthy, fixed-mouse DTI studies thus provide otherwise unattainable resolutions and associated directional information. Postnatal brain development in mice up to 80 days old has been monitored and analyzed using *ex vivo* DTI.¹¹⁷ Individual brain structures can be followed for changes in shape and volume. Studies of mutant mice in comparison to normal mice reveal regions of abnormal development, such as dysmyelination in the *Shiverer* mutant.¹¹⁸ In addition to studies in the brain, fixation has allowed accurate DTI mapping of fiber orientation in the mouse heart with implications for improved functional heart modeling.¹¹⁹ Such a study would be impractical *in vivo* in the mouse (although DTI in the beating human heart has been reported recently^{120,121}).

In addition to specimen and embryo imaging, large regions of the mouse or even whole-body, adult mouse images can be obtained following fixation. Imaging whole mice in this fashion has been termed magnetic resonance histology (MRH).¹²² MRH complements tra-

ditional two-dimensional histology with high-resolution, three-dimensional detail over the entire mouse. Perfusion fixation techniques have been developed that leave the mouse anatomy almost wholly undisturbed,^{123,124} so that *in situ* phenotype information can be derived from the entire mouse. High concentrations of a gadolinium contrast agent can be used in the perfusate to shorten the T_1 relaxation times of tissues for rapid gradient-echo imaging so that very high-resolution imaging can be conveniently run in an ‘overnight’ scanning session. Alternatively, T_2 -weighted imaging can be based on fast spin-echo pulse sequences and have been used for high-resolution imaging in fixed mice at the Toronto Mouse Imaging Centre. Such MRH techniques have also been used to create ‘The Visible Mouse’¹²³ shown in Fig. 8, a non-destructive visualization of the entire mouse at spatial resolution near 100 μm isotropic.

Cancer studies

Cancer studies merit special mention owing to the large number of studies in the literature and the important role of MRI as a non-invasive readout. There is a clear need to monitor tumor development longitudinally for progression or regression. Additionally, non-invasive appraisal of the relative state of tumor blood supply and also regions of viable or necrotic tissue greatly benefits longitudinal cancer studies. MRI is a powerful means of addressing these challenges.

Early cancer studies used subcutaneously implanted xenograft tumors to model cancer in humans. This is convenient because growth curves can be generated by simple caliper measurements and localization is trivial.

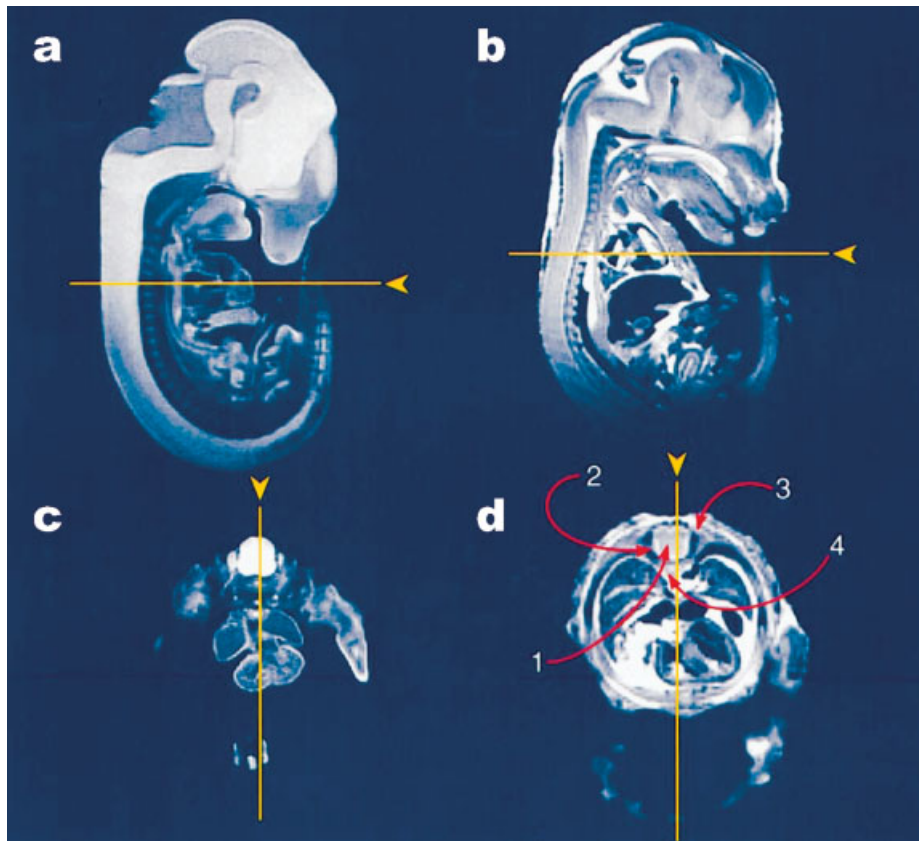


Figure 7. MRI atlas of fixed mouse embryos at 11.5 (a and c) and 15.5 (b and d) days post-conception (dpc). Sagittal (a and b) and transverse (c and d) sections are shown with orange lines indicating the location of each section. The 11.5 and 15.5 dpc embryos are collected with 19.5 and 39 μm isotropic voxels, respectively. Labels indicate the spinal cord (1), the marginal layer (2) (bright ring), the dorsal roots (3) (lateral dark regions) and the vertebral body primordium (4). Image courtesy of Dhenain *et al.*¹¹³ Reprinted from Reference 113 with permission from Elsevier

MRI contributes less to these studies as a result. Although these tumor models are simple and less physiologically realistic, they can be advantageous in MRI protocol development studies. For example, radiographic scoring¹²⁵ and multispectral analysis¹²⁶ techniques have been designed in subcutaneous xenograft models for differentiation of tumors into regions of viable tissue and necrosis. MR images have also been used to identify tumor regions and guide genomic analyses, yielding lists of upregulated genes in tumor regions identifiable by altered MR appearance.¹²⁷ Techniques of functional measurement in tumors can similarly be assayed and developed in these models.^{128–130} In the light of recent interest in anti-angiogenic therapies,^{131–134} imaging measures of tumor vasculature including contrast-enhanced imaging protocols^{135–138} are candidates for development.

A more realistic model of cancer is obtained by growing tumors in an appropriate tissue environment, preferably orthotopically. Implanting xenograft tumors deeper within tissues and organs throughout the body means that they will only be accessible *in vivo* by non-invasive imaging such as MRI. As mouse MRI techniques have improved, the number of studies using MRI to

monitor orthotopic xenograft models has also grown. Initial characterization of tumors in these models is important. As in clinical experience, tumor appearance on MRI varies. The presence of the growth factor VEGFA, for instance, has been shown to alter the appearance of human melanoma xenografts.¹³⁹ This may be advantageous, allowing inferences about the state of tumor blood supply or regions of tumor viability and necrosis. Similarly, tumor growth and morphology can be highly variable even within the same tumor model¹⁴⁰ – this can likewise be a desirable feature as it mimics the properties of human disease. Several examples of the characterization of tumor growth and/or evaluation of therapies in orthotopic models of pancreatic,^{141,142} bladder^{143–145} and brain^{140,146,147} tumors, among others, have been performed with mouse MRI. Functional MR methods for monitoring the vascular state of tissue and angiogenesis are also important in these models.^{148,149} In the GL261 glioma model, measures of relative cerebral blood volume compare well with histological measures of vascular density,¹⁴⁹ thus supporting *in vivo* MR measures in future studies. Images of cancer progression in this model are provided in Fig. 9.

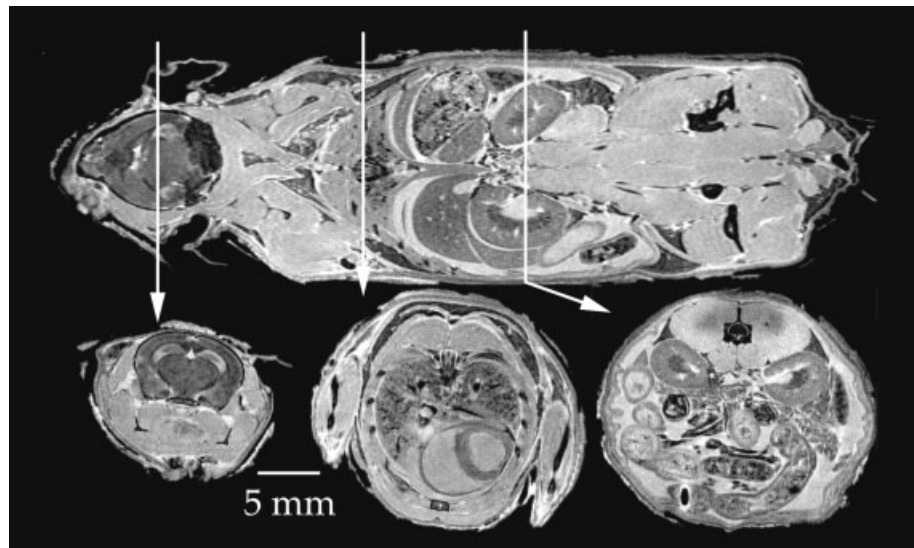


Figure 8. The visible Mouse generated by three-dimensional MRI of a whole fixed C57BL/6J mouse as described by Johnson *et al.*¹²³ The image was acquired with an isotropic array $256 \times 256 \times 1024$ with resolution $110 \times 110 \times 110 \mu\text{m}$. Coronal (top) and transverse (bottom) images depict sections of the head (left), thorax (center) and abdomen (right). Reprinted from Reference 123 with permission from the Radiological Society of North America

The study of spontaneously-developing murine tumors may be the most accurate model physiologically for understanding the disease processes of cancer. Heterogeneity in these models, including variable times of tumor onset and growth rates, is representative of the human disease but also poses challenges for analysis and biological interpretation. The aim of imaging in these studies is thus regular screening for detection of cancers followed by longitudinal monitoring of their progression. Mouse MRI can be used in this capacity. Initial studies have been used to characterize murine tumor models and compare them with the equivalent human cancer. One

study assessed the progression of prostate cancer in transgenic mice; identification of a heterogeneous yet persistent tumor development with variable times of onset and cancer death is consistent with the human disease.¹⁵⁰ Similarly, initial studies of a knockout model of gastric tumors¹⁵¹ and an ENU generated model of colon cancer¹⁵² have been reported with tumor detection and volume measurement by MRI. High-resolution, high-throughput *in vivo* MR imaging aids in overcoming the challenges associated with these experiments and will allow for more complete studies of spontaneously developing murine tumors in the future.

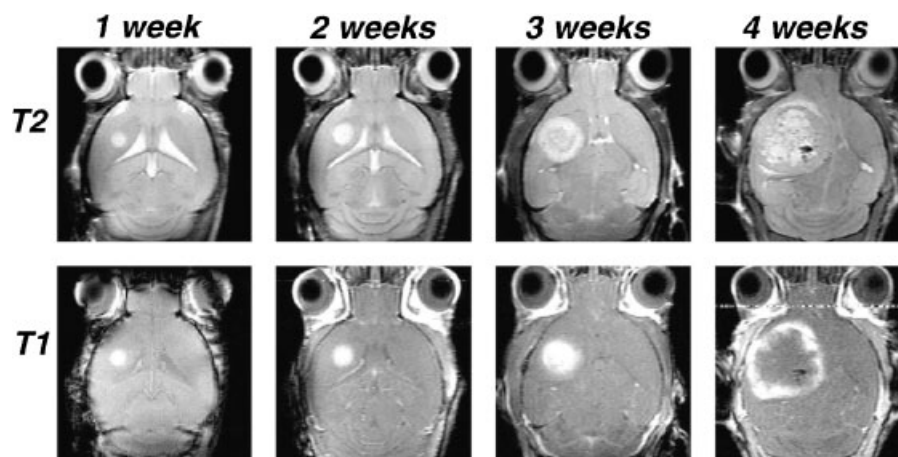


Figure 9. GL261 glioma progression as revealed with *in vivo* MRI by Cha *et al.*¹⁴⁹ Horizontal images from different mice at four time points are shown with precontrast T_2 -weighting (upper panels) and post-contrast T_1 -weighting (lower panels). T_2 signal intensity is observed to be increasingly heterogeneous with time, whereas post-contrast T_1 enhancement is confined by 4 weeks to the tumor rim. Reprinted from Reference 149 with permission from John Wiley & Sons, Inc.

MR spectroscopy

While this review is intended to focus on mouse phenotyping by MR imaging, MR spectroscopy is another tool for non-invasive assessment of mouse models. Similar human-to-mouse scale challenges are present in MRS as in MRI; volumes of interest are proportionately smaller and well-resolved spectra become more difficult to obtain. In addition to compounding existing time constraints in MRS, which is already more time consuming than MRI examinations, this may require specialized hardware such as custom high-order shim coils.¹⁵³ Much of the reported work has been performed in the larger rat as a result. However, the study of mouse models of human disease and screening in random mutagenesis trials can benefit from the development of 'metabolic phenotyping' in addition to image based techniques.

There are many human MRS methods (see Ross and Bluml¹⁵⁴ for a review). Only some of these have been adapted and used for localized *in vivo* spectroscopy in the mouse. Single-voxel ¹H MRS studies are the most common. They are frequently used in mouse models of brain diseases to quantify levels of *N*-acetylaspartate (NAA) and creatine (Cr) relative to choline (Co), but may also be used in monitoring levels of glutamate and glutamine (Glx), among other metabolites. Several mouse models have been assessed by these techniques. A recent review of *in vivo* MRS in neurodegenerative diseases¹⁵⁵ provides several examples including mouse models of amyotrophic lateral sclerosis and Huntington's disease. In other studies, mutant APP mice¹⁵⁶ and PS2APP mice¹⁵⁷ (expressing both APP and mutant human presenilin 2) exhibit decreased levels of NAA and glutamate and increased levels of taurine; this is consistent with similar findings in human cases of Alzheimer disease.¹⁵⁸ MRS methods are also well suited to the monitoring of Canavan disease, a neurodegenerative disease characterized as a deficiency in aspartoacylase and elevated levels of NAA.¹⁵⁹ Mouse models of this disease have been created¹⁶⁰ and preliminary research into genetic therapies use MRS to monitor *in vivo* NAA levels.¹⁶¹ Models and treatment of other inherited brain diseases studied by MRS are also cited in the literature.^{162–166}

Outside of the brain, *in vivo* studies have been performed in the heart and skeletal muscle.¹⁶⁷ These studies often report ³¹P MRS data as a marker of energy metabolism, which is remarkably well conserved across species from human to mouse.^{168,169} Differences in metabolism in myocardium between wild-type and transgenic mice expressing bovine growth hormone – expected to have a lower PCr to ATP ratio – have been demonstrated *in vivo*.¹⁷⁰ Other investigations have monitored the effects of ischemia in the presence of mice overexpressing A₃ adenosine receptors, showing improved preservation of ATP and a protective effect.¹⁷¹ This kind of *in vivo* metabolic study provides important insight into the process of heart disease and potential therapies.

If *in vivo* measurements are not necessary, the data drawn from individual samples in MRS studies can be greatly enhanced. MRS may benefit even more from *ex vivo* examinations than MRI in this regard. The energetics in the heart can be studied surprisingly well in this manner,^{172–175} although caution is warranted in interpretation of these results.¹⁷⁶ Hearts from genetically modified mice may show either an increased¹⁷⁷ or decreased¹⁷⁸ sensitivity to ischemic injury. Mouse models of Duchenne muscular dystrophy are an additional example.^{167,174,179,180} In addition to the study of *ex vivo* tissue, spectroscopy of biofluids can be used for screening and analysis of mice. This has the advantage that it can be done without ill effect to the mouse and even performed longitudinally if only small samples are required. A differential phenotype of two mouse strains has been achieved on the basis of high-resolution ¹H MRS of urine, for example.^{181,182} More details on these techniques have already been published.¹⁸³

KEEPING UP WITH BIOLOGICAL STUDIES: MULTIPLE MOUSE MR IMAGING

Although many of the techniques and developments in clinical MRI can be scaled to the mouse, as highlighted by the studies discussed above, it is important to recognize that there are several unique challenges in imaging mice for biomedical research. During any given day at a clinical human scanner, individual patients arrive with a selection of unrelated conditions that are each addressed by a different battery of imaging protocols. Each patient must therefore receive very specific attention. In mouse imaging, however, the philosophy at the scanner is different. A typical biological study requires *N* control mice and another *N* affected mice to be imaged in an identical manner so that results can be pooled and significant information drawn from the comprehensive data set. Within this data set, several types of images may be acquired and then may also be repeated at subsequent intervals to monitor progression. Furthermore, the power of a study improves with larger *N*. Hence an enormous amount of image data is typically collected and systematically processed. In mouse imaging, high-image throughput and protocol efficiency is essential for biological studies given typical constraints on MRI resources. Mouse phenotyping relies on systematic and efficient mouse image acquisition.

This philosophy shift to high-throughput, standardized imaging necessarily forces a streamlining of the image protocol. Running sessions one after another *N*-times faster is an inappropriate solution given the physical timing limitations in MRI, the need for high-resolution data and/or the time series data in functional experiments. An alternative solution is to run MRI sessions in parallel on multiple mice using multiple-mouse MRI (MMMRI). This solution was first described by Bock

et al.,¹⁸⁴ who examined the tradeoffs inherent in several different imaging configurations. Alternative magnet designs for dedicated MMMRI scanners continue to be explored.¹⁸⁵

The simplest MMMRI configuration to implement is to use a large radiofrequency coil with an appropriate size magnet and gradient to image several mice within the same field-of-view. As many as 17 mice have been imaged *in vivo* in this fashion on a standard clinical scanner.¹⁸⁶ Similarly, 32 fixed mouse embryos have been imaged at high resolution by this approach in a 12 h scan.¹⁸⁷ Following data acquisition, post-processing is required to separate individual mice from the combined image. Although this technique is the most straightforward to implement – virtually any clinical scanner can be used with little or no modification – degradation of image quality as compared with an optimized single mouse imaging configuration cannot be avoided.

An improved parallelization scheme is to supply an individual RF coil for each mouse but continue to use a common gradient coil. This maintains the sensitivity of using small single-sample RF coils and, with the use of shielding to isolate the individual coils, also allows the imaging field-of-view to be reduced to the size of a single mouse. Early demonstration of this technique on a 1.5 T clinical scanner was presented in fixed mice.¹⁸⁴ More recently, a longitudinal cancer study demonstrated imaging of seven mice at a time in a dedicated 7 T MMMRI scanner.¹⁴⁰ Sixteen fixed mice have also been imaged simultaneously. This three-dimensional, isotropic resolution data set is presented in Fig. 10. Post-processing of data sets in these studies requires individual reconstruction of each of the separate data sets. Additional field-of-view unwrapping due to phase encode aliasing in off-center samples may also be necessary; although phase control in the receiver hardware could be used to acquire the offset field-of-view directly on many MR scanners. These processing steps are easily automated. Some modification to scanner hardware is necessary, most notably an increased number of receivers and/or multiplexers routing single RF transmitter–receiver pairs to multiple RF coils. Fortunately, with the widespread use of SENSE and SMASH, scanners with multiple receivers are becoming commonplace. If there are as many receivers as mice, the only sacrifice over dedicated single mouse arrangements is the reduced performance inherent in a larger gradient.

The most complex MMMRI scheme implemented to date uses an individual RF coil for each mouse and a set of gradients sized for each mouse.¹⁸⁸ Custom gradient coils with a novel unshielded design are connected in series and run in synchrony. In principle, this greatly improves gradient performance over larger, full-bore gradient sets and approaches the dedicated single mouse coil case. This form of parallelization has been implemented to image eight fixed mouse fetuses simultaneously. Post-processing may require taking into

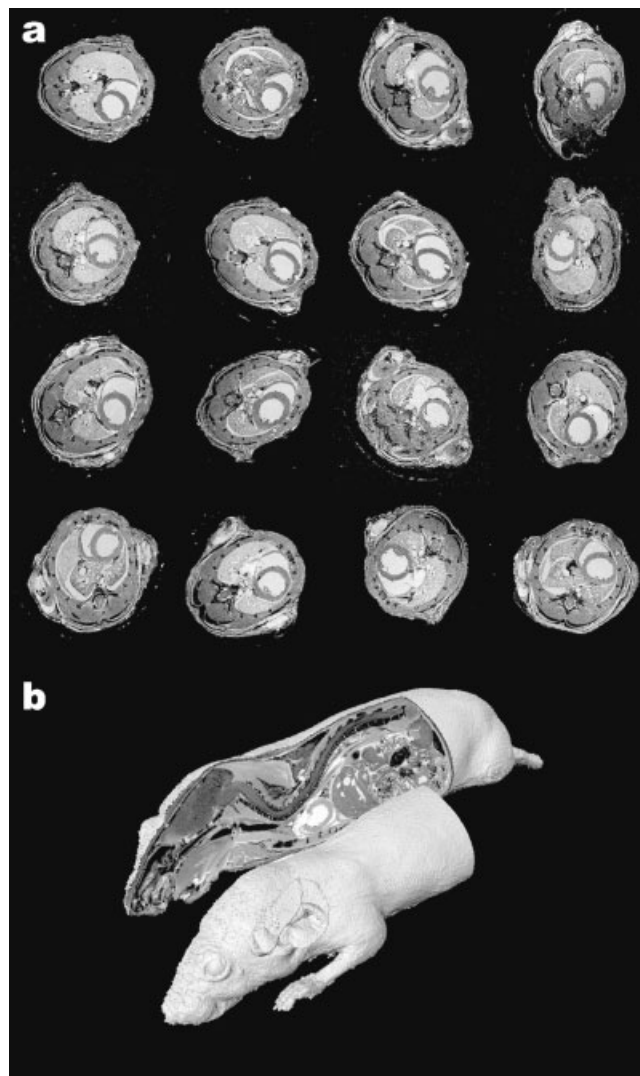


Figure 10. Multiple-mouse MRI data acquisition. In this data set, 16 fixed mice were imaged simultaneously in the same time required to image a single mouse. A slice through the thorax is shown in (a) for all individual mice. In (b), an individual mouse is surface rendered with cut-away planes showing the high-resolution, three-dimensional and isotropic nature of all 16 data sets

account slightly different gradient strengths at different positions. This configuration is the most difficult to implement in that significant hardware modification is necessary. Additionally, multiple gradient coil elements occupy a significant volume in the homogeneous region of the magnetic field, which reduces the degree of parallelization achieved.

Independent of the technique of image parallelization, mouse handling techniques and hardware must be developed to anesthetize and maintain the multiple mice over the course of an *in vivo* scan, as is true in single mouse MRI. These should likewise be parallelized to the extent possible to improve efficiency. All of the mice for a given scan session must first be anesthetized, attached to necessary monitoring equipment (which usually requires shaving and/or chemical hair removal) and placed in the

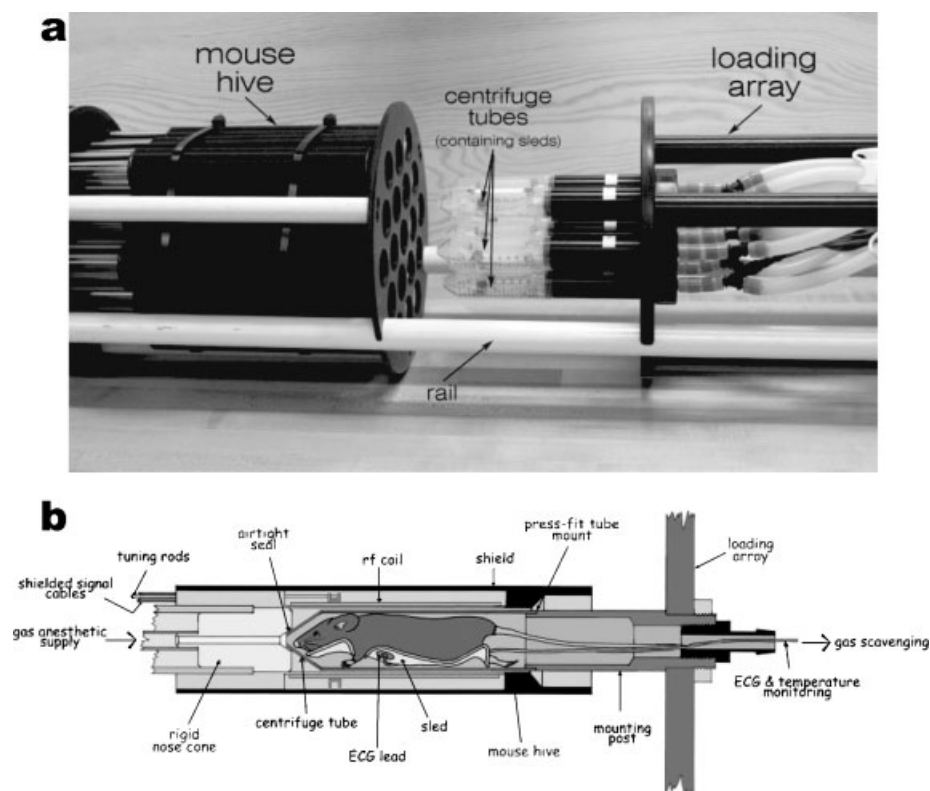


Figure 11. An efficient MMMRI loading system as described by Dazai *et al.*¹² In (a), a loading array equipped with anesthesia scavenging holds multiple mice in centrifuge tubes and is slid down rails into the ‘mouse hive’, which holds up to 19 RF transmit–receive coils. Mouse ‘sleds’ provide molded platforms for mouse positioning and on-board monitoring. A cut-away view in (b) shows the docking of one mouse into its RF coil in the mouse hive where isoflurane anesthetic is delivered by nose cone throughout the imaging experiment. Reprinted from Reference 12 with permission from John Wiley & Sons, Inc.

magnet and coil. Throughout the imaging experiment, vital signs must be monitored and adjustments made to maintain body temperature as needed. Figure 11 shows some of the handling hardware that we have implemented.¹² With this setup, as many as seven mice can be loaded for imaging in less than 30 min. Furthermore, the process can be extended to accommodate as many as 19 mice. Several alternative hardware configurations for positioning^{10,11} and monitoring^{189–192} have been reported for single mice. Mouse handling hardware and protocols of this kind greatly improve the efficiency of mouse MRI.

The entire MRI protocol and pulse sequence may also require modification as a consequence of parallelization. Ideally, one would like the flexibility of using any existing human protocol when examining the mouse. Several limitations may have to be considered, however. First, the prescan in MMMRI needs to be streamlined. Selection of specific slices of interest in multiple mice may be difficult and/or time consuming. It is therefore more time efficient to prescribe three-dimensional isotropic images with retrospective selection of the anatomy of interest. Interestingly, this may also become a strategy in clinical imaging with highly parallel SENSE configurations.¹⁹³ Second, in order to achieve the increased resolution for mouse MRI, the minimum duration of

gradient pulses increases. This extra delay is compensated for in dedicated mouse MR scanners through a decreased bore size and increased gradient strength. Finally, if there are fewer receivers than coils, extra time in the MR pulse sequence must be allowed for multiplexing of different RF coils. This dead time introduces restrictions that may prohibit use of some very rapid sequences. Within this context, we have presented an optimized FSE protocol for multiple mouse imaging.¹⁹⁴ This protocol attains 100 μm isotropic image resolution in multiple mice *in vivo* in 2 h 45 min of scanning as presented in Fig. 12. In most anatomical imaging experiments, pulse sequence design constraints are not a significant limitation of MMMRI.

The various forms of functional imaging are more difficult to parallelize, however. In these experiments, repeated images must usually be acquired during or following blocks of stimulus, contrast agent injections and/or physiological triggers for gating. Conceivably, some of these steps could be parallelized with hardware and/or protocol development (e.g. parallel application of electrical stimulus in fMRI). Perhaps the most challenging of these examples is gated imaging. In the absence of invasive cardiac pacing and intubation strategies, mice heartbeat and respiration events are asynchronous and

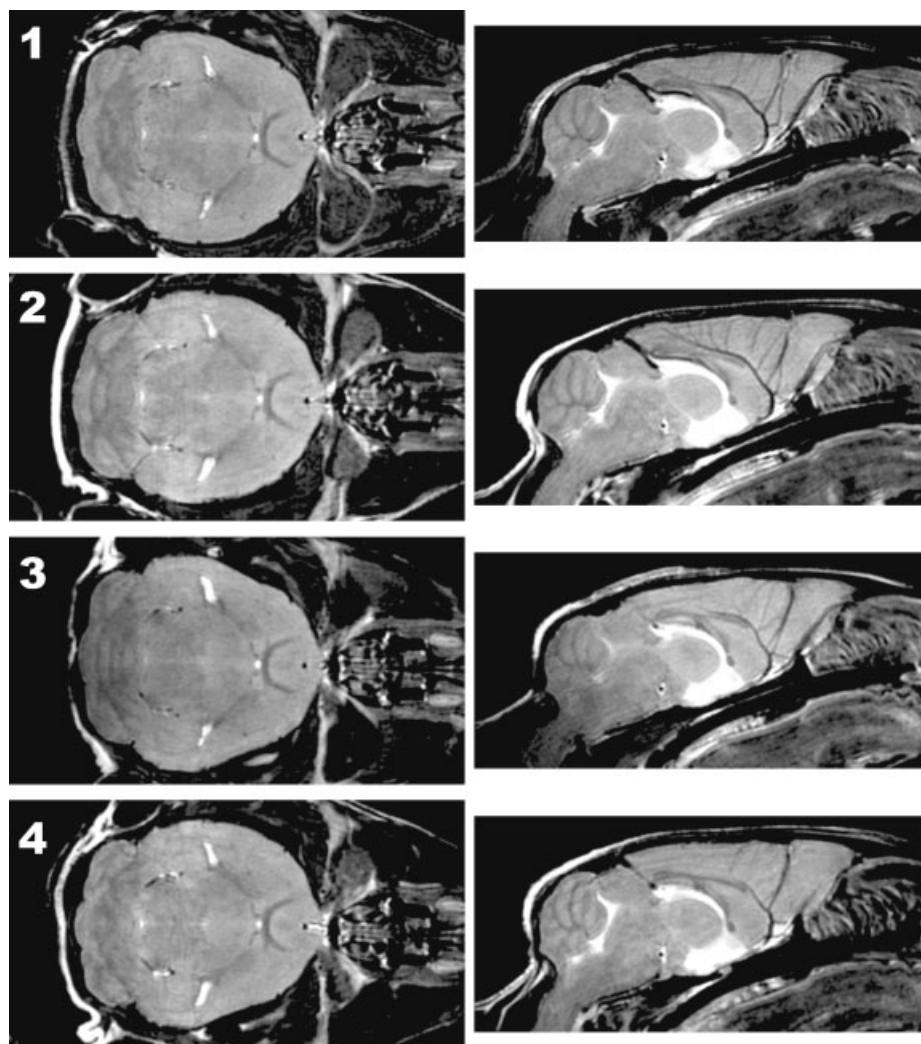


Figure 12. Coronal (left) and sagittal (right) slices from fast spin-echo MMMRI images of four mice. Each three-dimensional image is $100\ \mu\text{m}$ isotropic resolution. Scan duration was 2 h 50 min

prospectively gated image acquisitions are impossible. Acquisition of cine cardiac images for functional evaluation of the heart is thus compromised in multiple-mouse imaging configurations. One solution to this difficulty is retrospective gating. Since cardiac and respiratory monitoring of the mice is already a necessity even in ungated imaging protocols, the only enabling hardware/software developments required are the collection and storage of these signals for each mouse. These physiological data can then be used to reconstruct individually images gated for each mouse using retrospective reconstruction techniques. Initial proof-of-principle experiments in our laboratory on a single mouse compare well with prospective gating results in a single mouse at an increased time cost, similar to the performance of retrospective gating in human studies. Provided that the number of mice imaged in parallel exceeds the time cost, a significant efficiency advantage is still achieved. Development of these types of parallelized functional imaging protocols is ongoing.

If mouse MRI is to become a regular tool for biomedical research, it must be efficient in its application. The studies summarized here are means of producing an increased mouse throughput by parallelization of the imaging process. Before any studies are initiated, it is important to assess the number of mice that will be required to obtain satisfactory data. Large-scale screening experiments, pre-clinical trials or other large N experiments are impractical if long imaging sessions are required and only one mouse can be imaged at a time. In this regard, parallelization of image acquisitions represents an effective means of keeping up with biological studies.

ANALYSIS OF MULTIPLE-MOUSE ANATOMICAL DATA

Once a means of acquiring data for biological studies has been established, analysis of the data becomes a significant challenge. In some studies, such as in the

case of certain functional or quantitative measurements, a single scalar quantity of interest – the volume of a particular structure or the ejection fraction in the heart are examples – can be derived from individual images and then compared between groups of mice or serially over time. As comparisons across samples must be made only in anatomically relevant regions, this process can be greatly facilitated by image registration. Recent implementations of such analyses include the registration of images in an Alzheimer disease model in order to create an average T_2 map, resulting in an improved ability to distinguish local changes between experimental and control groups.¹⁹⁵ Such data analyses can provide not only improved spatial information but also temporal information. For example, DTI images of fixed brains can be registered at various stages of early development. The fractional anisotropy may then be used to characterize normal brain maturation.¹⁹⁶

In addition to scalar measures, the size and shape of anatomy itself is often interesting for phenotype characterization. However, in comparing normal and mutant mouse anatomy, the three-dimensional nature of the data must be maintained and evaluated over multiple images and multiple experimental groups. Analysis of these data sets thus requires representation of an ‘average’ anatomy with an assessment of the associated normal biological variation in local size and shape. An experimental group of mice can then be compared against this average and evaluated for outliers based on the established variability. The production of this sort of variational atlas has been reported for *ex vivo* mouse brains by our group.¹⁹⁷ This method uses registration and atlas generation algorithms

adapted from human studies.¹⁹⁸ As a result of the genetic homogeneity of subjects in mouse studies, very high-resolution data can be maintained even in the average image with the added benefits of improved SNR and reduced levels of artifact. The low level of biological variation within inbred strains also makes the identification of outliers much easier. Figure 13 offers an example of this averaging and atlas generation in the fixed mouse brain, showing the sample non-linear deformation grid for one of the mice that is required to form the overall average.

These analysis techniques are also intended to analyze *in vivo* and *in situ* data. We have recently collected *in vivo* neuroanatomical data from several different mutant mice generated from a random mutagenesis program in a secondary screening capacity. Mice with behavioral conditions or other symptoms that suggested possible brain abnormalities were selected for scanning using normal littermates as controls. Using the same analysis as for fixed brains, we have thus far observed an abnormal neuroanatomical phenotype in five of six heterozygous or homozygous mutants. This important observation suggests that anatomical abnormalities are important indications of genetic disease and frequently correlate with functional deficits. Figure 14 shows sample data of an average control and an average mutant mouse with a defect in the *Gjal* gene. The deformations required to produce the mutant brain from the control wild type are overlaid on the mutant average as a vector field. This mutant is a model for a rare human disease called oculodentodigital dysplasia.¹⁹⁹ Differences in brain shape and size were observed, most notably in the

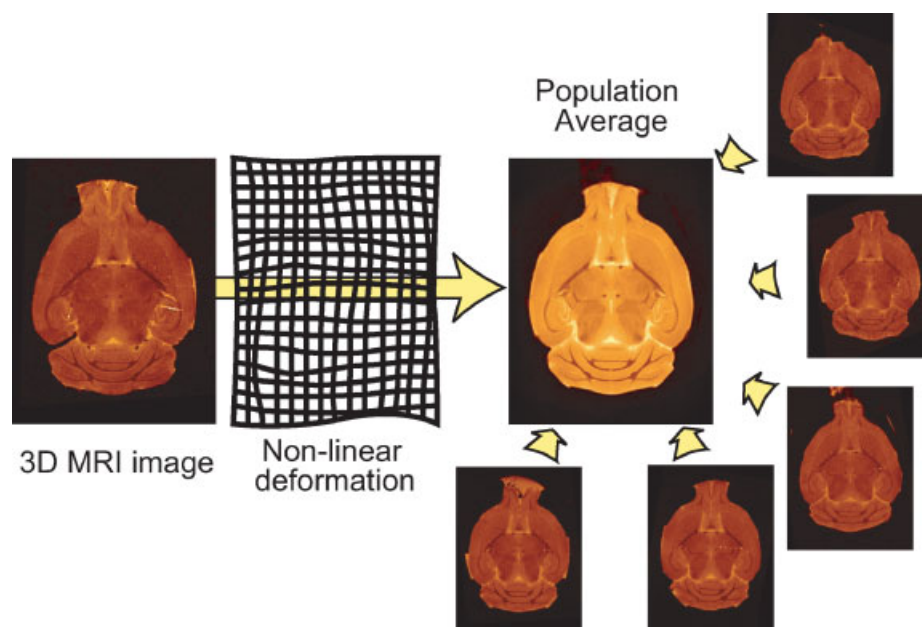


Figure 13. Non-linear deformation of fixed brains and generation of a population average. The average is chosen as an intermediate between all of the images, avoiding bias to a single member. Deformation fields (shown as a grid for one of the brains) map each individual to the average and encode the population variability

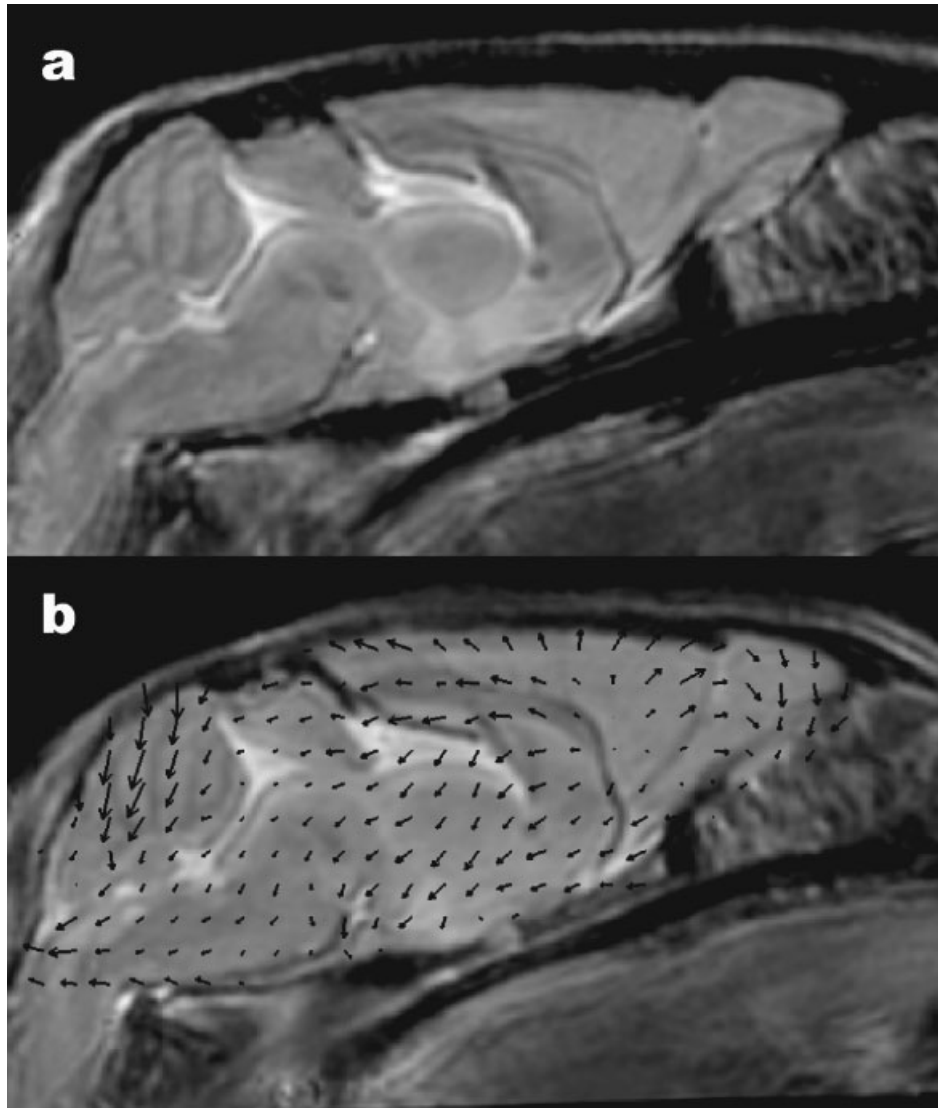


Figure 14. *In vivo* evaluation of an uncharacterized mutant. The average control image is shown in (a). The average *Gja1* mutant image is shown in (b) with an overlay of the deformation fields required to map the control into the mutant. The vectors are at $2 \times$ scale

cerebellum and the forebrain. In this case the data set was produced using a total of 10 mice, five mutants and five controls. We have performed similar *in vivo* data analysis in as many as 15 mice by similar methods. The volumes of particular brain structures can also be assessed by this method. In this case, the generation of a manually labeled atlas needs to be performed once, but then the transformations between each individual and the atlas may be used to measure volume differences between normal and mutant groups. This greatly improves the efficiency of the data analysis process necessary to characterize mutant anatomy.

Sophisticated imaging and analysis techniques are often required for the detection and quantification of abnormalities in uncharacterized mutant mice. In some cases, significant effort may be necessary in order to

customize existing registration and analysis protocols for a particular application. However, the resulting automated analysis package enables accelerated analysis of the many-image data sets typical to biological studies. We have found this can be achieved using the equivalent computing power of a single high-end workstation with minimal operator input. Future studies aimed at discovering, studying or comparing new mouse models to human diseases will inevitably depend on the use and development of these kinds of image analysis tools.

CONCLUSIONS

The needs to observe anatomical and functional changes *in vivo* and to produce high-resolution three-dimensional

visualizations have motivated a tremendous growth of mouse imaging in recent years. Mouse MRI is an impressive phenotyping tool enabling these studies. Many of the significant developments in human clinical MRI are being successfully transferred to small animal imaging and mouse-specific imaging developments are emerging. Extremely high-resolution scans of fixed mice also complement the information available from *in vivo* scans and traditional histology by offering superior three-dimensional visualization over the whole mouse.

Advances in multiple mouse techniques with the associated sequences and hardware are greatly increasing the efficiency of mouse MRI and making larger, more powerful biological studies possible. Consequently, mouse MRI is used increasingly in the study of mouse models of human disease and promises to make significant contributions in understanding mouse genetics and pathology. A detailed understanding of the genetic factors in mouse models of human diseases will revolutionize clinical medicine in this century – the ultimate goal of mouse phenotyping by MRI.

Acknowledgements

The authors gratefully acknowledge funding support from the Canada Foundation for Innovation/Ontario Innovation Trust, Ontario Research and Development Challenge Fund, National Institutes of Health, Canadian Institutes of Health Research, Genome Canada and the Burroughs Wellcome Fund. Brian Nieman is the recipient of a Canada Graduate Scholarship. Mark Henkelman is the recipient of a Canada Research Chair in Imaging.

REFERENCES

- International Human Genome Sequencing Consortium. Initial sequencing and analysis of the human genome. *Nature* 2001; **409**: 860–921.
- Mouse Genome Sequencing Consortium. Initial sequencing and comparative analysis of the mouse genome. *Nature* 2002; **420**: 520–562.
- van der WL, Adams DJ, Bradley A. Tools for targeted manipulation of the mouse genome. *Physiol Genomics* 2002; **11**: 133–164.
- Hrabe de Angelis MH, Flaswinkel H, Fuchs H, Rathkolb B, Soewarto D, Marschall S, Heffner S, Pargent W, Wuensch K, Jung M, Reis A, Richter T, Alessandrini F, Jakob T, Fuchs E, Kolb H, Kremmer E, Schaeble K, Rollinski B, Roscher A, Peters C, Meitinger T, Strom T, Steckler T, Holsboer F, Klopstock T, Gekeler F, Schindewolf C, Jung T, Avraham K, Behrendt H, Ring J, Zimmer A, Schughart K, Pfeffer K, Wolf E, Balling R. Genome-wide, large-scale production of mutant mice by ENU mutagenesis. *Nat. Genet.* 2000; **25**: 444–447.
- Nolan PM, Peters J, Strivens M, Rogers D, Hagan J, Spurr N, Gray IC, Vizor L, Brooker D, Whitehill E, Washbourne R, Hough T, Greenaway S, Hewitt M, Liu X, McCormack S, Pickford K, Selley R, Wells C, Tymowska-Lalanne Z, Roby P, Glenister P, Thornton C, Thaug C, Stevenson JA, Arkell R, Mburu P, Hardisty R, Kiernan A, Erven A, Steel KP, Voegelings S, Guenet JL, Nickols C, Sadri R, Nasse M, Isaacs A, Davies K, Browne M, Fisher EM, Martin J, Rastan S, Brown SD, Hunter J. A systematic, genome-wide, phenotype-driven mutagenesis programme for gene function studies in the mouse. *Nat. Genet.* 2000; **25**: 440–443.
- O'Brien TP, Frankel WN. Moving forward with chemical mutagenesis in the mouse. *J. Physiol.* 2004; **554**: 13–21.
- Hansen J, Floss T, Van Sloun P, Fuchtbauer EM, Vauti F, Arnold HH, Schnutgen F, Wurst W, von Melchner H, Ruiz P. A large-scale, gene-driven mutagenesis approach for the functional analysis of the mouse genome. *Proc. Natl. Acad. Sci. USA* 2003; **100**: 9918–9922.
- Stanford WL, Cohn JB, Cordes SP. Gene-trap mutagenesis: past, present and beyond. *Nat. Rev. Genet.* 2001; **2**: 756–768.
- Beck B, Plant DH, Grant SC, Thelwall PE, Silver X, Mareci TH, Benveniste H, Smith M, Collins C, Crozier S, Blackband SJ. Progress in high field MRI at the University of Florida. *MAGMA* 2002; **13**: 152–157.
- Tada T, Wendland M, Watson N, Kuriyama N, Kuriyama H, Roberts T, Burns M, Weiss W, Israel MA. A head holder for magnetic resonance imaging that allows the stereotaxic alignment of spontaneously occurring intracranial mouse tumors. *J. Neurosci. Methods* 2002; **116**: 1–7.
- Fricke ST, Vink R, Chiodo C, Cernak I, Ileva L, Faden AI. Consistent and reproducible slice selection in rodent brain using a novel stereotaxic device for MRI. *J. Neurosci. Methods* 2004; **136**: 99–102.
- Dazai J, Bock NA, Nieman BJ, Davidson LM, Henkelman RM, Chen XJ. Multiple mouse biological loading and monitoring system for MRI. *Magn. Reson. Med.* 2004; **52**: 709–715.
- Natt O, Watanabe T, Boretius S, Radulovic J, Frahm J, Michaelis T. High-resolution 3D MRI of mouse brain reveals small cerebral structures *in vivo*. *J. Neurosci. Methods* 2002; **120**: 203–209.
- Weiss C, Venkatasubramanian PN, Aguado AS, Power JM, Tom BC, Li L, Chen KS, Disterhoft JF, Wyrwicz AM. Impaired eyeblink conditioning and decreased hippocampal volume in PDAPP V717F mice. *Neurobiol. Dis.* 2002; **11**: 425–433.
- Kooy RF, Reyniers E, Verhoye M, Sijbers J, Bakker CE, Oostra BA, Willems PJ, Van der LA. Neuroanatomy of the fragile X knockout mouse brain studied using *in vivo* high resolution magnetic resonance imaging. *Eur. J. Hum. Genet.* 1999; **7**: 526–532.
- Dubowitz DJ, Tyszka JM, Sewry CA, Moats RA, Scadeng M, Dubowitz V. High resolution magnetic resonance imaging of the brain in the *dy/dy* mouse with merosin-deficient congenital muscular dystrophy. *Neuromuscul. Disord.* 2000; **10**: 292–298.
- Diez M, Schweinhardt P, Petersson S, Wang FH, Lavebratt C, Schalling M, Hokfelt T, Spenger C. MRI and *in situ* hybridization reveal early disturbances in brain size and gene expression in the megencephalic (*mceph/mceph*) mouse. *Eur. J. Neurosci.* 2003; **18**: 3218–3230.
- Laskowitz DT, Sheng H, Bart RD, Joyner KA, Roses AD, Warner DS. Apolipoprotein E-deficient mice have increased susceptibility to focal cerebral ischemia. *J. Cereb. Blood Flow Metab.* 1997; **17**: 753–758.
- McDaniel B, Sheng H, Warner DS, Hedlund LW, Benveniste H. Tracking brain volume changes in C57BL/6J and ApoE-deficient mice in a model of neurodegeneration: a 5-week longitudinal micro-MRI study. *Neuroimage* 2001; **14**: 1244–1255.
- Meyding-Lamade U, Lamade W, Kehm R, Knopf KW, Hess T, Gosztonyi G, Degen O, Hacke W. Herpes simplex virus encephalitis: cranial magnetic resonance imaging and neuropathology in a mouse model. *Neurosci. Lett.* 1998; **248**: 13–16.
- Meyding-Lamade UK, Lamade WR, Wildemann BT, Sartor K, Hacke W. Herpes simplex virus encephalitis: chronic progressive cerebral magnetic resonance imaging abnormalities in patients despite good clinical recovery. *Clin. Infect. Dis.* 1999; **28**: 148–149.
- Meyding-Lamade UK, Oberlinner C, Rau PR, Seyfer S, Heiland S, Sellner J, Wildemann BT, Lamade WR. Experimental herpes simplex virus encephalitis: a combination therapy of acyclovir and glucocorticoids reduces long-term magnetic resonance imaging abnormalities. *J. Neurovirol.* 2003; **9**: 118–125.
- Pirko I, Gamez J, Johnson AJ, Macura SI, Rodriguez M. Dynamics of MRI lesion development in an animal model of

- viral-induced acute progressive CNS demyelination. *Neuroimage* 2004; **21**: 576–582.
24. Preece NE, Amor S, Baker D, Gadian DG, O'Neill JK, Urenjak J. Experimental encephalomyelitis modulates inositol and taurine in the spinal cord of Biozzi mice. *Magn. Reson. Med.* 1994; **32**: 692–697.
 25. Thomas HC, Kapadia RD, Wells GI, Gresham AM, Sutton D, Solleveld HA, Sarkar SK, Dillon SB, Tal-Singer R. Differences in pathogenicity of herpes simplex virus serotypes 1 and 2 may be observed by histopathology and high-resolution magnetic resonance imaging in a murine encephalitis model. *J. Neurovirol.* 2001; **7**: 105–116.
 26. Natt O, Watanabe T, Boretius S, Frahm J, Michaelis T. Magnetization transfer MRI of mouse brain reveals areas of high neural density. *Magn. Reson. Imaging* 2003; **21**: 1113–1120.
 27. Duvvuri U, Poptani H, Feldman M, Nadal-Desbarats L, Gee MS, Lee WM, Reddy R, Leigh JS, Glickson JD. Quantitative T1rho magnetic resonance imaging of RIF-1 tumors *in vivo*: detection of early response to cyclophosphamide therapy. *Cancer Res.* 2001; **61**: 7747–7753.
 28. Engelhardt RT, Johnson GA. T1 rho relaxation and its application to MR histology. *Magn. Reson. Med.* 1996; **35**: 781–786.
 29. Neufeld A, Eliav U, Navon G. New MRI method with contrast based on the macromolecular characteristics of tissues. *Magn. Reson. Med.* 2003; **50**: 229–234.
 30. Helpem JA, Lee SP, Falangola MF, Dyakin VV, Bogart A, Ardekani B, Duff K, Branch C, Wisniewski T, de Leon MJ, Wolf O, O'Shea J, Nixon RA. MRI assessment of neuropathology in a transgenic mouse model of Alzheimer's disease. *Magn. Reson. Med.* 2004; **51**: 794–798.
 31. Helpem JA, Jensen J, Lee SP, Falangola MF. Quantitative MRI assessment of Alzheimer's disease. *J. Mol. Neurosci.* 2004; **24**: 45–48.
 32. Song SK, Sun SW, Ramsbottom MJ, Chang C, Russell J, Cross AH. Demyelination revealed through MRI as increased radial (but unchanged axial) diffusion of water. *Neuroimage* 2002; **17**: 1429–1436.
 33. Xue R, Sawada M, Goto S, Hurn PD, Traystman RJ, van Zijl PC, Mori S. Rapid three-dimensional diffusion MRI facilitates the study of acute stroke in mice. *Magn. Reson. Med.* 2001; **46**: 183–188.
 34. Aden U, Dahlberg V, Fredholm BB, Lai LJ, Chen Z, Bjelke B. MRI evaluation and functional assessment of brain injury after hypoxic ischemia in neonatal mice. *Stroke* 2002; **33**: 1405–1410.
 35. Mueggler T, Meyer-Luehmann M, Rausch M, Staufenbiel M, Jucker M, Rudin M. Restricted diffusion in the brain of transgenic mice with cerebral amyloidosis. *Eur. J. Neurosci.* 2004; **20**: 811–817.
 36. Song SK, Kim JH, Lin SJ, Brendza RP, Holtzman DM. Diffusion tensor imaging detects age-dependent white matter changes in a transgenic mouse model with amyloid deposition. *Neurobiol. Dis.* 2004; **15**: 640–647.
 37. Silva AC, Lee JH, Aoki I, Koretsky AP. Manganese-enhanced magnetic resonance imaging (MEMRI): methodological and practical considerations. *NMR Biomed.* 2004; **17**: 532–543.
 38. Aoki I, Wu YJ, Silva AC, Lynch RM, Koretsky AP. *In vivo* detection of neuroarchitecture in the rodent brain using manganese-enhanced MRI. *Neuroimage* 2004; **22**: 1046–1059.
 39. Wadghiri YZ, Blind JA, Duan X, Moreno C, Yu X, Joyner AL, Turnbull DH. Manganese-enhanced magnetic resonance imaging (MEMRI) of mouse brain development. *NMR Biomed.* 2004; **17**: 613–619.
 40. Watanabe T, Natt O, Boretius S, Frahm J, Michaelis T. *In vivo* 3D MRI staining of mouse brain after subcutaneous application of MnCl₂. *Magn. Reson. Med.* 2002; **48**: 852–859.
 41. Pautler RG. *In vivo*, trans-synaptic tract-tracing utilizing manganese-enhanced magnetic resonance imaging (MEMRI). *NMR Biomed.* 2004; **17**: 595–601.
 42. Watanabe T, Radulovic J, Spiess J, Natt O, Boretius S, Frahm J, Michaelis T. *In vivo* 3D MRI staining of the mouse hippocampal system using intracerebral injection of MnCl₂. *Neuroimage* 2004; **22**: 860–867.
 43. Poduslo JF, Wengenack TM, Curran GL, Wisniewski T, Sigurdsson EM, Macura SI, Borowski BJ, Jack CR Jr. Molecular targeting of Alzheimer's amyloid plaques for contrast-enhanced magnetic resonance imaging. *Neurobiol. Dis.* 2002; **11**: 315–329.
 44. Wadghiri YZ, Sigurdsson EM, Sadowski M, Elliott JI, Li Y, Scholtzova H, Tang CY, Aguinaldo G, Pappolla M, Duff K, Wisniewski T, Turnbull DH. Detection of Alzheimer's amyloid in transgenic mice using magnetic resonance microimaging. *Magn. Reson. Med.* 2003; **50**: 293–302.
 45. Jack CR, Jr., Garwood M, Wengenack TM, Borowski B, Curran GL, Lin J, Adriany G, Grohn OH, Grimm R, Poduslo JF. *In vivo* visualization of Alzheimer's amyloid plaques by magnetic resonance imaging in transgenic mice without a contrast agent. *Magn. Reson. Med.* 2004; **52**: 1263–1271.
 46. Lee SP, Falangola MF, Nixon RA, Duff K, Helpem JA. Visualization of beta-amyloid plaques in a transgenic mouse model of Alzheimer's disease using MR microscopy without contrast reagents. *Magn. Reson. Med.* 2004; **52**: 538–544.
 47. Zhang J, Yarowsky P, Gordon MN, Di CG, Munireddy S, van Zijl PC, Mori S. Detection of amyloid plaques in mouse models of Alzheimer's disease by magnetic resonance imaging. *Magn. Reson. Med.* 2004; **51**: 452–457.
 48. Zeligyanskaya ML, Nelson JA, Poluektova L, Uberti M, Mellon M, Gendelman HE, Boska MD. Tracking superparamagnetic iron oxide labeled monocytes in brain by high-field magnetic resonance imaging. *J. Neurosci. Res.* 2003; **73**: 284–295.
 49. Anderson SA, Glod J, Arbab AS, Noel M, Ashari P, Fine HA, Frank JA. Noninvasive MR imaging of magnetically labeled stem cells to directly identify neovasculature in a glioma model. *Blood* 2005; **105**: 420–425.
 50. Anderson SA, Shukaliak-Quandt J, Jordan EK, Arbab AS, Martin R, McFarland H, Frank JA. Magnetic resonance imaging of labeled T-cells in a mouse model of multiple sclerosis. *Ann. Neurol.* 2004; **55**: 654–659.
 51. Moore A, Grimm J, Han B, Santamaria P. Tracking the recruitment of diabetogenic CD8+ T-cells to the pancreas in real time. *Diabetes* 2004; **53**: 1459–1466.
 52. Smirnov P, Gazeau F, Lewin M, Bacri JC, Siauve N, Vayssettes C, Cuenod CA, Clement O. *In vivo* cellular imaging of magnetically labeled hybridomas in the spleen with a 1.5-T clinical MRI system. *Magn. Reson. Med.* 2004; **52**: 73–79.
 53. Himes N, Min JY, Lee R, Brown C, Shea J, Huang X, Xiao YF, Morgan JP, Burstein D, Oettgen P. *In vivo* MRI of embryonic stem cells in a mouse model of myocardial infarction. *Magn. Reson. Med.* 2004; **52**: 1214–1219.
 54. Zhao M, Kircher MF, Josephson L, Weissleder R. Differential conjugation of tat peptide to superparamagnetic nanoparticles and its effect on cellular uptake. *Bioconjug. Chem* 2002; **13**: 840–844.
 55. Hinds KA, Hill JM, Shapiro EM, Laukkanen MO, Silva AC, Combs CA, Varney TR, Balaban RS, Koretsky AP, Dunbar CE. Highly efficient endosomal labeling of progenitor and stem cells with large magnetic particles allows magnetic resonance imaging of single cells. *Blood* 2003; **102**: 867–872.
 56. Kircher MF, Allport JR, Graves EE, Love V, Josephson L, Lichtman AH, Weissleder R. *In vivo* high resolution three-dimensional imaging of antigen-specific cytotoxic T-lymphocyte trafficking to tumors. *Cancer Res.* 2003; **63**: 6838–6846.
 57. Sipe JC, Filippi M, Martino G, Furlan R, Rocca MA, Rovaris M, Bergami A, Zyroff J, Scotti G, Comi G. Method for intracellular magnetic labeling of human mononuclear cells using approved iron contrast agents. *Magn. Reson. Imaging* 1999; **17**: 1521–1523.
 58. Arbab AS, Yocum GT, Kalish H, Jordan EK, Anderson SA, Khakoo AY, Read EJ, Frank JA. Efficient magnetic cell labeling with protamine sulfate complexed to ferumoxides for cellular MRI. *Blood* 2004; **104**: 1217–1223.
 59. Deans AE, Yu X, Wadghiri YZ, Duan XC, Turnbull DH. 7 T-MRI of transferrin receptor and ferritin gene expression in a mouse neural stem cell line. Presented at the International Society for Magnetic Resonance in Medicine 13th Scientific Meeting, May 2005, Miami Beach, FL.
 60. Weissleder R, Lee AS, Khaw BA, Shen T, Brady TJ. Antimyosin-labeled monocrySTALLINE iron oxide allows detection of myocardial infarct: MR antibody imaging. *Radiology* 1992; **182**: 381–385.

61. Kang HW, Josephson L, Petrovsky A, Weissleder R, Bogdanov A Jr. Magnetic resonance imaging of inducible E-selectin expression in human endothelial cell culture. *Bioconjug. Chem* 2002; **13**: 122–127.
62. Artemov D, Mori N, Okollie B, Bhujwalla ZM. MR molecular imaging of the Her-2/neu receptor in breast cancer cells using targeted iron oxide nanoparticles. *Magn. Reson. Med.* 2003; **49**: 403–408.
63. So PW, Hotee S, Herlihy AH, Bell JD. MRI-based generic method for imaging transgene expression. Presented at the International Society for Magnetic Resonance in Medicine 13th Scientific Meeting, May 200, Miami Beach, FL.
64. Changani KK, Nicholson A, White A, Latham JK, Reid DG, Clapham JC. A longitudinal magnetic resonance imaging (MRI) study of differences in abdominal fat distribution between normal mice and lean overexpressors of mitochondrial uncoupling protein-3 (UCP-3). *Diabetes Obesity Metab.* 2002; **5**: 99–105.
65. Jo SK, Hu X, Kobayashi H, Lizak M, Miyaji T, Koretsky A, Star RA. Detection of inflammation following renal ischemia by magnetic resonance imaging. *Kidney Int.* 2003; **64**: 43–51.
66. Kobayashi H, Kawamoto S, Jo SK, Sato N, Saga T, Hiraga A, Konishi J, Hu S, Togashi K, Brechbiel MW, Star RA. Renal tubular damage detected by dynamic micro-MRI with a dendrimer-based magnetic resonance contrast agent. *Kidney Int.* 2002; **61**: 1980–1985.
67. Kobayashi H, Kawamoto S, Brechbiel MW, Jo SK, Hu X, Yang T, Diwan BA, Waldmann TA, Schnermann J, Choyke PL, Star RA. Micro-MRI methods to detect renal cysts in mice. *Kidney Int.* 2004; **65**: 1511–1516.
68. Bonny JM, Gaviria M, Donnat JP, Jean B, Privat A, Renou JP. Nuclear magnetic resonance microimaging of mouse spinal cord *in vivo*. *Neurobiol. Dis.* 2004; **15**: 474–482.
69. Dardzinski BJ, Schmithorst VJ, Holland SK, Boivin GP, Imagawa T, Watanabe S, Lewis JM, Hirsch R. MR imaging of murine arthritis using ultrasmall superparamagnetic iron oxide particles. *Magn. Reson. Imaging* 2001; **19**: 1209–1216.
70. Munasinghe JP, Tyler JA, Carpenter TA, Hall LD. High resolution MR imaging of joint degeneration in the knee of the STR/ORT mouse. *Magn. Reson. Imaging* 1995; **13**: 421–428.
71. Beckmann N, Gentsch C, Baumann D, Bruttel K, Vassout A, Schoeffter P, Loetscher E, Bobadilla M, Perentes E, Rudin M. Non-invasive, quantitative assessment of the anatomical phenotype of corticotropin-releasing factor-overexpressing mice by MRI. *NMR Biomed.* 2001; **14**: 210–216.
72. Choudhury RP, Fuster V, Fayad ZA. Molecular, cellular and functional imaging of atherothrombosis. *Nat. Rev. Drug Discov.* 2004; **3**: 913–925.
73. Chaabane L, Soulas EC, Contard F, Salah A, Guerrier D, Briguet A, Douek P. High-resolution magnetic resonance imaging at 2 Tesla: potential for atherosclerotic lesions exploration in the apolipoprotein E knockout mouse. *Invest. Radiol.* 2003; **38**: 532–538.
74. Choudhury RP, Aguinaldo JG, Rong JX, Kulak JL, Kulak AR, Reis ED, Fallon JT, Fuster V, Fisher EA, Fayad ZA. Atherosclerotic lesions in genetically modified mice quantified *in vivo* by non-invasive high-resolution magnetic resonance microscopy. *Atherosclerosis* 2002; **162**: 315–321.
75. Fayad ZA, Fallon JT, Shinnar M, Wehrli S, Dansky HM, Poon M, Badimon JJ, Charlton SA, Fisher EA, Breslow JL, Fuster V. Noninvasive *in vivo* high-resolution magnetic resonance imaging of atherosclerotic lesions in genetically engineered mice. *Circulation* 1998; **98**: 1541–1547.
76. Wiesmann F, Szimtenings M, Frydrychowicz A, Illinger R, Hunecke A, Rommel E, Neubauer S, Haase A. High-resolution MRI with cardiac and respiratory gating allows for accurate *in vivo* atherosclerotic plaque visualization in the murine aortic arch. *Magn. Reson. Med.* 2003; **50**: 69–74.
77. Choudhury RP, Fayad ZA, Aguinaldo JG, Itskovich VV, Rong JX, Fallon JT, Fisher EA. Serial, noninvasive, *in vivo* magnetic resonance microscopy detects the development of atherosclerosis in apolipoprotein E-deficient mice and its progression by arterial wall remodeling. *J. Magn. Reson. Imaging* 2003; **17**: 184–189.
78. Trogan E, Fayad ZA, Itskovich VV, Aguinaldo JG, Mani V, Fallon JT, Cheresnev I, Fisher EA. Serial studies of mouse atherosclerosis by *in vivo* magnetic resonance imaging detect lesion regression after correction of dyslipidemia. *Arterioscler. Thromb. Vasc. Biol.* 2004; **24**: 1714–1719.
79. Hockings PD, Roberts T, Galloway GJ, Reid DG, Harris DA, Vidgeon-Hart M, Groot PH, Suckling KE, Benson GM. Repeated three-dimensional magnetic resonance imaging of atherosclerosis development in innominate arteries of low-density lipoprotein receptor-knockout mice. *Circulation* 2002; **106**: 1716–1721.
80. Manka DR, Gilson W, Sarembock I, Ley K, Berr SS. Non-invasive *in vivo* magnetic resonance imaging of injury-induced neointima formation in the carotid artery of the apolipoprotein-E null mouse. *J. Magn. Reson. Imaging* 2000; **12**: 790–794.
81. Itskovich VV, Choudhury RP, Aguinaldo JG, Fallon JT, Omerhodzic S, Fisher EA, Fayad ZA. Characterization of aortic root atherosclerosis in ApoE knockout mice: high-resolution *in vivo* and ex vivo MRM with histological correlation. *Magn. Reson. Med.* 2003; **49**: 381–385.
82. Baudalet C, Gallez B. Effect of anesthesia on the signal intensity in tumors using BOLD-MRI: comparison with flow measurements by laser Doppler flowmetry and oxygen measurements by luminescence-based probes. *Magn. Reson. Imaging* 2004; **22**: 905–912.
83. van Dorsten FA, Hata R, Maeda K, Franke C, Eis M, Hossmann KA, Hoehn M. Diffusion- and perfusion-weighted MR imaging of transient focal cerebral ischaemia in mice. *NMR Biomed.* 1999; **12**: 525–534.
84. Hoehn M, Nicolay K, Franke C, van der SB. Application of magnetic resonance to animal models of cerebral ischemia. *J. Magn. Reson. Imaging* 2001; **14**: 491–509.
85. Kokubo Y, Matson GB, Derugin N, Hill T, Mancuso A, Chan PH, Weinstein PR. Transgenic mice expressing human copper-zinc superoxide dismutase exhibit attenuated apparent diffusion coefficient reduction during reperfusion following focal cerebral ischemia. *Brain Res.* 2002; **947**: 1–8.
86. Fabry ME, Kennan RP, Paszty C, Costantini F, Rubin EM, Gore JC, Nagel RL. Magnetic resonance evidence of hypoxia in a homozygous alpha-knockout of a transgenic mouse model for sickle cell disease. *J. Clin. Invest* 1996; **98**: 2450–2455.
87. Kennan RP, Suzuka SM, Nagel RL, Fabry ME. Decreased cerebral perfusion correlates with increased BOLD hyperoxia response in transgenic mouse models of sickle cell disease. *Magn. Reson. Med.* 2004; **51**: 525–532.
88. Wu EX, Tang H, Asai T, Yan SD. Regional cerebral blood volume reduction in transgenic mutant APP (V717F, K670N/M671L) mice. *Neurosci. Lett.* 2004; **365**: 223–227.
89. Mueggler T, Sturchler-Pierrat C, Baumann D, Rausch M, Staufenbiel M, Rudin M. Compromised hemodynamic response in amyloid precursor protein transgenic mice. *J. Neurosci.* 2002; **22**: 7218–7224.
90. Beckmann N, Schuler A, Mueggler T, Meyer EP, Wiederhold KH, Staufenbiel M, Krucker T. Age-dependent cerebrovascular abnormalities and blood flow disturbances in APP23 mice modeling Alzheimer's disease. *J. Neurosci.* 2003; **23**: 8453–8459.
91. Ahrens ET, Dubowitz DJ. Peripheral somatosensory fMRI in mouse at 11.7 T. *NMR Biomed.* 2001; **14**: 318–324.
92. Nair G, Duong TQ. Echo-planar BOLD fMRI of mice on a narrow-bore 9.4 T magnet. *Magn. Reson. Med.* 2004; **52**: 430–434.
93. Mueggler T, Baumann D, Rausch M, Staufenbiel M, Rudin M. Age-dependent impairment of somatosensory response in the amyloid precursor protein 23 transgenic mouse model of Alzheimer's disease. *J. Neurosci.* 2003; **23**: 8231–8236.
94. Mueggler T, Baumann D, Rausch M, Rudin M. Biccuculline-induced brain activation in mice detected by functional magnetic resonance imaging. *Magn. Reson. Med.* 2001; **46**: 292–298.
95. Pautler RG, Koretsky AP. Tracing odor-induced activation in the olfactory bulbs of mice using manganese-enhanced magnetic resonance imaging. *Neuroimage* 2002; **16**: 441–448.
96. Xu F, Liu N, Kida I, Rothman DL, Hyder F, Shepherd GM. Odor maps of aldehydes and esters revealed by functional MRI

- in the glomerular layer of the mouse olfactory bulb. *Proc. Natl Acad. Sci. USA* 2003; **100**: 11029–11034.
97. Ruff J, Wiesmann F, Lanz T, Haase A. Magnetic resonance imaging of coronary arteries and heart valves in a living mouse: techniques and preliminary results. *J. Magn. Reson.* 2000; **146**: 290–296.
 98. Wiesmann F, Ruff J, Hiller KH, Rommel E, Haase A, Neubauer S. Developmental changes of cardiac function and mass assessed with MRI in neonatal, juvenile and adult mice. *Am. J. Physiol. Heart Circ. Physiol.* 2000; **278**: H652–H657.
 99. Nahrendorf M, Hiller KH, Hu K, Ertl G, Haase A, Bauer WR. Cardiac magnetic resonance imaging in small animal models of human heart failure. *Med. Image Anal.* 2003; **7**: 369–375.
 100. Ross AJ, Yang Z, Berr SS, Gilson WD, Petersen WC, Oshinski JN, French BA. Serial MRI evaluation of cardiac structure and function in mice after reperfused myocardial infarction. *Magn. Reson. Med.* 2002; **47**: 1158–1168.
 101. Schneider JE, Hulbert K, Lygate CA, Hove MT, Cassidy PJ, Clarke K, Neubauer S. Long-term stability of cardiac function in normal and chronically failing mouse hearts in a vertical-bore MR system. *MAGMA* 2004; **17**: 162–169.
 102. Wiesmann F, Frydrychowicz A, Rautenberg J, Illinger R, Rommel E, Haase A, Neubauer S. Analysis of right ventricular function in healthy mice and a murine model of heart failure by *in vivo* MRI. *Am. J. Physiol. Heart Circ. Physiol.* 2002; **283**: H1065–H1071.
 103. Schneider JE, Cassidy PJ, Lygate C, Tyler DJ, Wiesmann F, Grieve SM, Hulbert K, Clarke K, Neubauer S. Fast, high-resolution *in vivo* cine magnetic resonance imaging in normal and failing mouse hearts on a vertical 11.7 T system. *J. Magn. Reson. Imaging* 2003; **18**: 691–701.
 104. Williams SP, Gerber HP, Giordano FJ, Peale FV Jr, Bernstein LJ, Bunting S, Chien KR, Ferrara N, Van BN. Dobutamine stress cine-MRI of cardiac function in the hearts of adult cardiomyocyte-specific VEGF knockout mice. *J. Magn. Reson. Imaging* 2001; **14**: 374–382.
 105. Wiesmann F, Ruff J, Engelhardt S, Hein L, Dienesch C, Leupold A, Illinger R, Frydrychowicz A, Hiller KH, Rommel E, Haase A, Lohse MJ, Neubauer S. Dobutamine-stress magnetic resonance microimaging in mice: acute changes of cardiac geometry and function in normal and failing murine hearts. *Circ. Res.* 2001; **88**: 563–569.
 106. Hu TC, Pautler RG, MacGowan GA, Koretsky AP. Manganese-enhanced MRI of mouse heart during changes in inotropy. *Magn. Reson. Med.* 2001; **46**: 884–890.
 107. Hu TC, Bao W, Lenhard SC, Schaeffer TR, Yue TL, Willette RN, Jucker BM. Simultaneous assessment of left-ventricular infarction size, function and tissue viability in a murine model of myocardial infarction by cardiac manganese-enhanced magnetic resonance imaging (MEMRI). *NMR Biomed.* 2004; **17**: 620–626.
 108. Zhou R, Pickup S, Glickson JD, Scott CH, Ferrari VA. Assessment of global and regional myocardial function in the mouse using cine and tagged MRI. *Magn. Reson. Med.* 2003; **49**: 760–764.
 109. Gilson WD, Yang Z, French BA, Epstein FH. Complementary displacement-encoded MRI for contrast-enhanced infarct detection and quantification of myocardial function in mice. *Magn. Reson. Med.* 2004; **51**: 744–752.
 110. Epstein FH, Yang Z, Gilson WD, Berr SS, Kramer CM, French BA. MR tagging early after myocardial infarction in mice demonstrates contractile dysfunction in adjacent and remote regions. *Magn. Reson. Med.* 2002; **48**: 399–403.
 111. Chapon C, Franconi F, Roux J, Marescaux L, Le Jeune JJ, Lemaire L. *In utero* time-course assessment of mouse embryo development using high resolution magnetic resonance imaging. *Anat. Embryol. (Berl.)* 2002; **206**: 131–137.
 112. Hogers B, Gross D, Lehmann V, Zick K, De Groot HJ, Gittenberger-De Groot AC, Poelmann RE. Magnetic resonance microscopy of mouse embryos *in utero*. *Anat. Rec.* 2000; **260**: 373–377.
 113. Dhenain M, Ruffins SW, Jacobs RE. Three-dimensional digital mouse atlas using high-resolution MRI. *Dev. Biol.* 2001; **232**: 458–470.
 114. Schneider JE, Bamforth SD, Grieve SM, Clarke K, Bhattacharya S, Neubauer S. High-resolution, high-throughput magnetic resonance imaging of mouse embryonic anatomy using a fast gradient-echo sequence. *MAGMA* 2003; **16**: 43–51.
 115. Guilfoyle DN, Helpert JA, Lim KO. Diffusion tensor imaging in fixed brain tissue at 7.0 T. *NMR Biomed.* 2003; **16**: 77–81.
 116. Sun SW, Neil JJ, Song SK. Relative indices of water diffusion anisotropy are equivalent in live and formalin-fixed mouse brains. *Magn. Reson. Med.* 2003; **50**: 743–748.
 117. Zhang J, Miller MI, Yarowsky P, van Zijl P, Mori S. Mapping postnatal mouse brain development with diffusion tensor microimaging. *Neuroimage* 2005; **26**: 1042–1051.
 118. Tyszkaj JM, Readhead C, Bearer EL, Pautler RG, Fraser SE, Jacobs RE. Statistical diffusion tensor histology reveals regional dysmyelination effects in the Shiverer mouse mutant. *Neuroimage* 2005; in press.
 119. Jiang Y, Pandya K, Smithies O, Hsu EW. Three-dimensional diffusion tensor microscopy of fixed mouse hearts. *Magn. Reson. Med.* 2004; **52**: 453–460.
 120. Dou J, Reese TG, Tseng WY, Wedeen VJ. Cardiac diffusion MRI without motion effects. *Magn. Reson. Med.* 2002; **48**: 105–114.
 121. Dou J, Tseng WY, Reese TG, Wedeen VJ. Combined diffusion and strain MRI reveals structure and function of human myocardial laminar sheets *in vivo*. *Magn. Reson. Med.* 2003; **50**: 107–113.
 122. Johnson GA, Cofer GP, Fubara B, Gewalt SL, Hedlund LW, Maronpot RR. Magnetic resonance histology for morphologic phenotyping. *J. Magn. Reson. Imaging* 2002; **16**: 423–429.
 123. Johnson GA, Cofer GP, Gewalt SL, Hedlund LW. Morphologic phenotyping with MR microscopy: the visible mouse. *Radiology* 2002; **222**: 789–793.
 124. Zhou YQ, Davidson L, Henkelman RM, Nieman BJ, Foster FS, Yu LX, Chen XJ. Ultrasound-guided left-ventricular catheterization: a novel method of whole mouse perfusion for microimaging. *Lab. Invest.* 2004; **84**: 385–389.
 125. Yang YS, Guccione S, Bednarski MD. Comparing genomic and histologic correlations to radiographic changes in tumors: a murine SCC VII model study. *Acad. Radiol.* 2003; **10**: 1165–1175.
 126. Carano RA, Ross AL, Ross J, Williams SP, Koeppen H, Schwall RH, Van BN. Quantification of tumor tissue populations by multispectral analysis. *Magn. Reson. Med.* 2004; **51**: 542–551.
 127. Guccione S, Yang YS, Shi G, Lee DY, Li KC, Bednarski MD. Functional genomics guided with MR imaging: mouse tumor model study. *Radiology* 2003; **228**: 560–568.
 128. Kim YR, Savellano MD, Savellano DH, Weissleder R, Bogdanov A Jr. Measurement of tumor interstitial volume fraction: method and implication for drug delivery. *Magn. Reson. Med.* 2004; **52**: 485–494.
 129. Marzola P, Farace P, Calderan L, Crescimanno C, Lunati E, Nicolato E, Benati D, Degrossi A, Terron A, Klapwijk J, Pesenti E, Sbarbati A, Osculati F. *In vivo* mapping of fractional plasma volume (fpv) and endothelial transfer coefficient (Kps) in solid tumors using a macromolecular contrast agent: correlation with histology and ultrastructure. *Int. J. Cancer* 2003; **104**: 462–468.
 130. Zhou R, Pickup S, Yankeelov TE, Springer CS Jr, Glickson JD. Simultaneous measurement of arterial input function and tumor pharmacokinetics in mice by dynamic contrast enhanced imaging: effects of transcytolemmal water exchange. *Magn. Reson. Med.* 2004; **52**: 248–257.
 131. Ferrara N, Alitalo K. Clinical applications of angiogenic growth factors and their inhibitors. *Nat. Med.* 1999; **5**: 1359–1364.
 132. Isayeva T, Kumar S, Ponnazhagan S. Anti-angiogenic gene therapy for cancer (review). *Int. J. Oncol.* 2004; **25**: 335–343.
 133. Purow B, Fine HA. Progress report on the potential of angiogenesis inhibitors for neuro-oncology. *Cancer Invest.* 2004; **22**: 577–587.
 134. Tortora G, Melisi D, Ciardiello F. Angiogenesis: a target for cancer therapy. *Curr. Pharm. Des.* 2004; **10**: 11–26.

135. Checkley D, Tessier JJ, Wedge SR, Dukes M, Kendrew J, Curry B, Middleton B, Waterton JC. Dynamic contrast-enhanced MRI of vascular changes induced by the VEGF-signalling inhibitor ZD4190 in human tumour xenografts. *Magn. Reson. Imaging* 2003; **21**: 475–482.
136. Pradel C, Siauve N, Bruneteau G, Clement O, de BC, Frouin F, Wedge SR, Tessier JL, Robert PH, Frijia G, Cuenod CA. Reduced capillary perfusion and permeability in human tumour xenografts treated with the VEGF signalling inhibitor ZD4190: an *in vivo* assessment using dynamic MR imaging and macromolecular contrast media. *Magn. Reson. Imaging* 2003; **21**: 845–851.
137. Marzola P, Degrassi A, Calderan L, Farace P, Crescimanno C, Nicolato E, Giusti A, Pesenti E, Terron A, Sbarbati A, Abrams T, Murray L, Osculati F. *In vivo* assessment of antiangiogenic activity of SU6668 in an experimental colon carcinoma model. *Clin. Cancer Res.* 2004; **10**: 739–750.
138. Lewin M, Bredow S, Sergejev N, Marecos E, Bogdanov A Jr, Weissleder R. *In vivo* assessment of vascular endothelial growth factor-induced angiogenesis. *Int. J. Cancer* 1999; **83**: 798–802.
139. Leenders W, Kusters B, Pikkemaat J, Wesseling P, Ruitter D, Heerschap A, Barentsz J, de Waal RM. Vascular endothelial growth factor-A determines detectability of experimental melanoma brain metastasis in GD-DTPA-enhanced MRI. *Int. J. Cancer* 2003; **105**: 437–443.
140. Bock NA, Zadeh G, Davidson LM, Qian B, Sled JG, Guha A, Henkelman RM. High-resolution longitudinal screening with magnetic resonance imaging in a murine brain cancer model. *Neoplasia* 2003; **5**: 546–554.
141. Grimm J, Pothast A, Wunder A, Moore A. Magnetic resonance imaging of the pancreas and pancreatic tumors in a mouse orthotopic model of human cancer. *Int. J. Cancer* 2003; **106**: 806–811.
142. He Z, Evelhoch JL, Mohammad RM, Adsay NV, Pettit GR, Vaitkevicius VK, Sarkar FH. Magnetic resonance imaging to measure therapeutic response using an orthotopic model of human pancreatic cancer. *Pancreas* 2000; **21**: 69–76.
143. Kadhim SA, Chin JL, Batislam E, Karlik SJ, Garcia B, Skamene E. Genetically regulated response to intravesical bacillus Calmette Guerin immunotherapy of orthotopic murine bladder tumor. *J. Urol.* 1997; **158**: 646–652.
144. Kikuchi E, Xu S, Ohori M, Matei C, Lupu M, Menendez S, Koutcher JA, Bochner BH. Detection and quantitative analysis of early stage orthotopic murine bladder tumor using *in vivo* magnetic resonance imaging. *J. Urol.* 2003; **170**: 1375–1378.
145. Mazurchuk R, Glaves D, Raghavan D. Magnetic resonance imaging of response to chemotherapy in orthotopic xenografts of human bladder cancer. *Clin. Cancer Res.* 1997; **3**: 1635–1641.
146. Nelson AL, Algon SA, Munasinghe J, Graves O, Goumnerova L, Burstein D, Pomeroy SL, Kim JY. Magnetic resonance imaging of patched heterozygous and xenografted mouse brain tumors. *J. Neurooncol.* 2003; **62**: 259–267.
147. Rubin JB, Kung AL, Klein RS, Chan JA, Sun Y, Schmidt K, Kieran MW, Luster AD, Segal RA. A small-molecule antagonist of CXCR4 inhibits intracranial growth of primary brain tumors. *Proc. Natl Acad. Sci. USA* 2003; **100**: 13513–13518.
148. Thomas CD, Chenu E, Walczak C, Plessis MJ, Perin F, Volk A. Morphological and carbonogen-based functional MRI of a chemically induced liver tumor model in mice. *Magn. Reson. Med.* 2003; **50**: 522–530.
149. Cha S, Johnson G, Wadghiri YZ, Jin O, Babb J, Zagzag D, Turnbull DH. Dynamic, contrast-enhanced perfusion MRI in mouse gliomas: correlation with histopathology. *Magn. Reson. Med.* 2003; **49**: 848–855.
150. Hsu CX, Ross BD, Chrisp CE, Derrow SZ, Charles LG, Pienta KJ, Greenberg NM, Zeng Z, Sanda MG. Longitudinal cohort analysis of lethal prostate cancer progression in transgenic mice. *J. Urol.* 1998; **160**: 1500–1505.
151. Berr SS, Roche JK, El-Rifai W, Smith MF Jr, Powell SM. Magnetic resonance imaging of gastric cancer in Tff1 knock-out mice. *Magn. Reson. Med.* 2003; **49**: 1033–1036.
152. Hensley HH, Chang WC, Clapper ML. Detection and volume determination of colonic tumors in Min mice by magnetic resonance micro-imaging. *Magn. Reson. Med.* 2004; **52**: 524–529.
153. Tkac I, Henry PG, Andersen P, Keene CD, Low WC, Gruetter R. Highly resolved *in vivo* 1H NMR spectroscopy of the mouse brain at 9.4 T. *Magn. Reson. Med.* 2004; **52**: 478–484.
154. Ross B, Bluml S. Magnetic resonance spectroscopy of the human brain. *Anat. Rec.* 2001; **265**: 54–84.
155. Choi IY, Lee SP, Guilfoyle DN, Helpert JA. *In vivo* NMR studies of neurodegenerative diseases in transgenic and rodent models. *Neurochem. Res.* 2003; **28**: 987–1001.
156. Dedeoglu A, Choi JK, Cormier K, Kowall NW, Jenkins BG. Magnetic resonance spectroscopic analysis of Alzheimer's disease mouse brain that express mutant human APP shows altered neurochemical profile. *Brain Res.* 2004; **1012**: 60–65.
157. von KM, Kunnecke B, Metzger F, Steiner G, Richards JG, Ozmen L, Jacobsen H, Loetscher H. Altered metabolic profile in the frontal cortex of PS2APP transgenic mice, monitored throughout their life span. *Neurobiol. Dis.* 2005; **18**: 32–39.
158. Shonk TK, Moats RA, Gifford P, Michaelis T, Mandigo JC, Izumi J, Ross BD. Probable Alzheimer disease: diagnosis with proton MR spectroscopy. *Radiology* 1995; **195**: 65–72.
159. Matalon R, Michals K, Sebesta D, Deanching M, Gashkoff P, Casanova J. Aspartoacylase deficiency and *N*-acetylaspatic aciduria in patients with Canavan disease. *Am. J. Med. Genet.* 1988; **29**: 463–471.
160. Matalon R, Rady PL, Platt KA, Skinner HB, Quast MJ, Campbell GA, Matalon K, Ceci JD, Tying SK, Nehls M, Surendran S, Wei J, Ezell EL, Szucs S. Knock-out mouse for Canavan disease: a model for gene transfer to the central nervous system. *J. Gene Med.* 2000; **2**: 165–175.
161. Matalon R, Surendran S, Rady PL, Quast MJ, Campbell GA, Matalon KM, Tying SK, Wei J, Peden CS, Ezell EL, Muzyczka N, Mandel RJ. Adeno-associated virus-mediated aspartoacylase gene transfer to the brain of knockout mouse for canavan disease. *Mol. Ther.* 2003; **7**: 580–587.
162. Hesselbarth D, Franke C, Hata R, Brinker G, Hoehn-Berlage M. High resolution MRI and MRS: a feasibility study for the investigation of focal cerebral ischemia in mice. *NMR Biomed.* 1998; **11**: 423–429.
163. Huang W, Galdzicki Z, van GP, Balbo A, Chikhale EG, Schapiro MB, Rapoport SI. Brain myo-inositol level is elevated in Ts65Dn mouse and reduced after lithium treatment. *Neuroreport* 2000; **11**: 445–448.
164. 't Zandt HJ, Renema WK, Streijger F, Jost C, Klomp DW, Oerlemans F, Van der Zee CE, Wieringa B, Heerschap A. Cerebral creatine kinase deficiency influences metabolite levels and morphology in the mouse brain: a quantitative *in vivo* 1H and 31P magnetic resonance study. *J. Neurochem.* 2004; **90**: 1321–1330.
165. Lee WT, Chang C. Magnetic resonance imaging and spectroscopy in assessing 3-nitropropionic acid-induced brain lesions: an animal model of Huntington's disease. *Prog. Neurobiol.* 2004; **72**: 87–110.
166. Schwarcz A, Natt O, Watanabe T, Boretius S, Frahm J, Michaelis T. Localized proton MRS of cerebral metabolite profiles in different mouse strains. *Magn. Reson. Med.* 2003; **49**: 822–827.
167. Cole MA, Rafael JA, Taylor DJ, Lodi R, Davies KE, Styles P. A quantitative study of bioenergetics in skeletal muscle lacking troponin and dystrophin. *Neuromuscul. Disord.* 2002; **12**: 247–257.
168. Chacko VP, Aresta F, Chacko SM, Weiss RG. MRI/MRS assessment of *in vivo* murine cardiac metabolism, morphology and function at physiological heart rates. *Am. J. Physiol. Heart Circ. Physiol.* 2000; **279**: H2218–H2224.
169. Naumova AV, Weiss RG, Chacko VP. Regulation of murine myocardial energy metabolism during adrenergic stress studied by *in vivo* 31P NMR spectroscopy. *Am. J. Physiol. Heart Circ. Physiol.* 2003; **285**: H1976–H1979.
170. Omerovic E, Basetti M, Bollano E, Bohlooly M, Tornell J, Isgaard J, Hjalmarson A, Soussi B, Waagstein F. *In vivo* metabolic imaging of cardiac bioenergetics in transgenic mice. *Biochem. Biophys. Res. Commun.* 2000; **271**: 222–228.

171. Cross HR, Murphy E, Black RG, Auchampach J, Steenbergen C. Overexpression of A(3) adenosine receptors decreases heart rate, preserves energetics and protects ischemic hearts. *Am. J. Physiol. Heart Circ. Physiol.* 2002; **283**: H1562–H1568.
172. Burgess SC, Babcock EE, Jeffrey FM, Sherry AD, Malloy CR. NMR indirect detection of glutamate to measure citric acid cycle flux in the isolated perfused mouse heart. *FEBS Lett.* 2001; **505**: 163–167.
173. Saupe KW, Spindler M, Tian R, Ingwall JS. Impaired cardiac energetics in mice lacking muscle-specific isoenzymes of creatine kinase. *Circ. Res.* 1998; **82**: 898–907.
174. Skrabek RQ, Anderson JE. Metabolic shifts and myocyte hypertrophy in deflazacort treatment of mdx mouse cardiomyopathy. *Muscle Nerve* 2001; **24**: 192–202.
175. Wunderlich C, Fogel U, Godecke A, Heger J, Schrader J. Acute inhibition of myoglobin impairs contractility and energy state of iNOS-overexpressing hearts. *Circ. Res.* 2003; **92**: 1352–1358.
176. Kass DA, Hare JM, Georgakopoulos D. Murine cardiac function: a cautionary tail. *Circ. Res.* 1998; **83**: 1215–1223.
177. Cross HR, Lu L, Steenbergen C, Philipson KD, Murphy E. Overexpression of the cardiac Na⁺/Ca²⁺ exchanger increases susceptibility to ischemia/reperfusion injury in male, but not female, transgenic mice. *Circ. Res.* 1998; **83**: 1215–1223.
178. Tian R, Miao W, Spindler M, Javadpour MM, McKinney R, Bowman JC, Buttrick PM, Ingwall JS. Long-term expression of protein kinase C in adult mouse hearts improves postischemic recovery. *Proc. Natl Acad. Sci. USA* 1999; **96**: 13536–13541.
179. Griffin JL, Sang E, Evens T, Davies K, Clarke K. Metabolic profiles of dystrophin and utrophin expression in mouse models of Duchenne muscular dystrophy. *FEBS Lett.* 2002; **530**: 109–116.
180. McIntosh L, Granberg KE, Briere KM, Anderson JE. Nuclear magnetic resonance spectroscopy study of muscle growth, mdx dystrophy and glucocorticoid treatments: correlation with repair. *NMR Biomed.* 1998; **11**: 1–10.
181. Gavaghan CL, Holmes E, Lenz E, Wilson ID, Nicholson JK. An NMR-based metabolomic approach to investigate the biochemical consequences of genetic strain differences: application to the C57BL10J and Alpk:ApfCD mouse. *FEBS Lett.* 2000; **484**: 169–174.
182. Gavaghan CL, Wilson ID, Nicholson JK. Physiological variation in metabolic phenotyping and functional genomic studies: use of orthogonal signal correction and PLS-DA. *FEBS Lett.* 2002; **530**: 191–196.
183. Griffin JL. Metabolic profiles to define the genome: can we hear the phenotypes? *Philos. Trans. R. Soc. Lond. B Biol. Sci.* 2004; **359**: 857–871.
184. Bock NA, Konyer NB, Henkelman RM. Multiple-mouse MRI. *Magn. Reson. Med.* 2003; **49**: 158–167.
185. Ungersma SE, Scott GC, van Oort JM, Conolly SM. Magnet design considerations for parallel mouse imaging. Presented at the *Twelfth Scientific Meeting and Exhibition*, International Society for Magnetic Resonance in Medicine, May 2004, Kyoto.
186. Xu S, Gade TP, Matei C, Zakian K, Alfieri AA, Hu X, Holland EC, Soghomonian S, Tjuvajev J, Ballon D, Koutcher JA. *In vivo* multiple-mouse imaging at 1.5 T. *Magn. Reson. Med.* 2003; **49**: 551–557.
187. Schneider JE, Bose J, Bamforth SD, Gruber AD, Broadbent C, Clarke K, Neubauer S, Lengeling A, Bhattacharya S. Identification of cardiac malformations in mice lacking Ptdsr using a novel high-throughput magnetic resonance imaging technique. *BMC Dev. Biol.* 2004; **4**: 16.
188. Matsuda Y, Utsuzawa S, Kurimoto T, Haishi T, Yamazaki Y, Kose K, Anno I, Marutani M. Super-parallel MR microscope. *Magn. Reson. Med.* 2003; **50**: 183–189.
189. Fishbein KW, McConville P, Spencer RG. The lever-coil: a simple, inexpensive sensor for respiratory and cardiac motion in MRI experiments. *Magn. Reson. Imaging* 2001; **19**: 881–889.
190. Brau AC, Wheeler CT, Hedlund LW, Johnson GA. Fiber-optic stethoscope: a cardiac monitoring and gating system for magnetic resonance microscopy. *Magn. Reson. Med.* 2002; **47**: 314–321.
191. Cassidy PJ, Schneider JE, Grieve SM, Lygate C, Neubauer S, Clarke K. Assessment of motion gating strategies for mouse magnetic resonance at high magnetic fields. *J. Magn. Reson. Imaging* 2004; **19**: 229–237.
192. Garbow JR, Dugas JP, Song SK, Conradi MS. A simple, robust hardware device for passive or active respiratory gating in MRI and MRS experiments. *Concepts Magn. Reson.* 2004; **21B**: 40–48.
193. Sodickson D. Massively parallel MRI. Presented at the *Second International Workshop on Parallel MRI*, October 2004, Zurich.
194. Nieman BJ, Bock NA, Bishop J, Sled JG, Chen XJ, Henkelman RM. Fast spin-echo for multiple mouse MR phenotyping. *Magn. Reson. Med.* 2005; **54**: 532–537.
195. Falangola MF, Ardekani BA, Lee SP, Babb JS, Bogart A, Dyakin VV, Nixon R, Duff K, Helpert JA. Application of a non-linear image registration algorithm to quantitative analysis of T2 relaxation time in transgenic mouse models of AD pathology. *J. Neurosci. Methods* 2005; **144**: 91–97.
196. Verma R, Mori S, Shen D, Yarowsky P, Zhang J, Davatzikos C. Spatiotemporal maturation patterns of murine brain quantified by diffusion tensor MRI and deformation-based morphometry. *Proc. Natl. Acad. Sci. USA* 2005; **102**: 6978–6983.
197. Kovacevic N, Henderson JT, Chan E, Lifshitz N, Bishop J, Evans AC, Henkelman RM, Chen XJ. A three-dimensional MRI atlas of the mouse brain with estimates of the average and variability. *Cereb. Cortex* 2005; **15**: 639–645.
198. Joshi S, Davis B, Jomier M, Gerig G. Unbiased diffeomorphic atlas construction for computational anatomy. *Neuroimage* 2004; **23**(Suppl. 1): S151–S160.
199. Paznekas WA, Boyadjiev SA, Shapero RE, Daniels O, Wollnik B, Keegan CE, Innis JW, Dinulos MB, Christian C, Hannibal MC, Jabs EW. Connexin 43 (GJA1) mutations cause the pleiotropic phenotype of oculodentodigital dysplasia. *Am. J. Hum. Genet.* 2003; **72**: 408–418.